

ESCAPE RATES IN A STOCHASTIC ENVIRONMENT WITH MULTIPLE SCALES

ERIC FORGOSTON* AND IRA B. SCHWARTZ†

Abstract. We consider a stochastic environment with two time scales and outline a general theory that compares two methods to reduce the dimension of the original system. The first method involves the computation of the underlying deterministic center manifold followed by a “naïve” replacement of the stochastic term. The second method allows one to more accurately describe the stochastic effects and involves the derivation of a normal form coordinate transform that is used to find the stochastic center manifold. The results of both methods are used along with the path integral formalism of large fluctuation theory to predict the escape rate from one basin of attraction to another. The general theory is applied to the example of a surface flow described by a generic, singularly perturbed, damped, nonlinear oscillator with additive, Gaussian noise. We show how both nonlinear reduction methods compare in escape rate scaling. Additionally, the center manifolds are shown to predict high pre-history probability regions of escape. The theoretical results are confirmed using numerical computation of the mean escape time and escape prehistory, and we briefly discuss the extension of the theory to stochastic control.

Key words. Stochastic dynamical systems, Center manifold reduction, Large fluctuation theory, Multiscale analysis

AMS subject classifications. 37H10, 60H10, 93E03

1. Introduction. It has long been known that noise can have a significant effect on deterministic dynamical systems. For example, given an initial state starting in some basin of attraction (defined as the set of initial conditions from which the system approaches a corresponding locally stable attractor as time evolves to infinity), noise can cause the initial state to cross the basin boundary and move into another, distinct basin of attraction [12, 14, 39, 36, 35].

There are several points of view one might consider when investigating the effect of noise on a dynamical system, including stochastic resonance [24] and finite noise effects [5]. In this article, we consider yet another point of view, namely the effect of arbitrarily small noise on the escape of a particle from a potential well. In this case, one can apply large fluctuation theory [20, 12, 14, 36].

Many of the underlying deterministic systems found in [12, 14, 39, 36, 35] have parameter regimes in which multiple attractors give rise to noise-induced escape from one attractor to another. Such systems may be analyzed globally by considering the Hamiltonian theory of large fluctuations or by considering escape from attracting potential wells along most probable exit paths [23, 26, 37, 28].

Through the use of a path integral coupled with variational methods, it is possible to compute the probability densities of the trajectories of the system. In particular, for sufficiently small noise, one can find the trajectories which escape from a basin of attraction due to stochastic effects. The most probable escape trajectory is the optimal escape path of a state residing in a basin of attraction.

Many researchers have investigated how noise affects physical and biological phenomena, including lasers [8, 32, 27], epidemics and control [4, 17, 33, 16], and neurons [30]. Yet another important application in many fields is that of sensing in

*Nonlinear Dynamical Systems Section, Plasma Physics Division, Code 6792, U.S. Naval Research Laboratory, Washington, DC 20375, USA (eric.forgoston.ctr@nrl.navy.mil).

†Nonlinear Dynamical Systems Section, Plasma Physics Division, Code 6792, U.S. Naval Research Laboratory, Washington, DC 20375, USA (ira.schwartz@nrl.navy.mil).

stochastic environments. Improved environmental sensing and prediction can be achieved through the incorporation of continuous monitoring of the region of interest. For example, one could monitor the stochastic ocean using autonomous underwater gliders [48, 47, 19]. However, to do this, one must understand both the dynamics and control of the gliders.

Extending the lifetime (energy optimization problem) of sensing devices (e.g. gliders) in stochastic environments such as the ocean requires an understanding of the effect of the environmental forces on both the devices and the region being monitored. The ocean dynamics are high-dimensional and stochastic. Therefore, as a first step towards using the underlying ocean structure to optimize a sensor's energy usage, we will outline a general theory that provides two methods to obtain a reduction in the dimension of the stochastic system. The manifold equations that are found using these methods can then be used to determine the optimal escape path and escape rate.

Our formulation uses large fluctuation theory [20] to determine the first passage times in a multi-scale environment. For a vector field that has relaxation times on the same scale, it is clear how to use the theory to generate an optimal path of escape, and this theory has been applied to a variety of Hamiltonian and Lagrangian variational problems [49, 31, 15].

However, technical issues may arise when one wishes to determine the projection of noise that is needed to perturb the dynamics restricted to the lower-dimensional manifold. To address this, several approaches have been developed to understand dimension reduction in systems that have well separated time scales. For a system with certain spectral requirements, the existence of a stochastic center manifold was proven in [6]. Non-rigorous stochastic normal form analysis (which leads to the stochastic center manifold) was performed in [34, 9, 40, 41]. Rigorous theoretical analysis of normal form coordinate transformations for stochastic center manifold reduction was developed in [2, 1]. Later, an alternative method of stochastic normal form reduction was developed [42], in which any anticipatory convolutions (integrals into the future of the noise processes) that appeared in the slow modes were removed. Since this latter analysis makes the construction of the stochastic normal form coordinate transform more transparent, we use this method to derive the reduced stochastic center manifold equation.

The layout of the paper is as follows. The general theory of deterministic and stochastic center manifold reduction is described in Sec. 2. The first method used to reduce the dimension of the system involves the derivation of the center manifold equation [7] of the associated deterministic system followed by the “naïve” replacement of the stochastic term. The second method, which allows one to more accurately describe the effect of the noise, involves the derivation of a normal form coordinate transform [42] that is used to find the stochastic center manifold equation. Section 2 also describes how the two center manifolds resulting from the two methods can be used along with the theory of large fluctuations to analytically find the optimal escape path of the particle along with its escape rate. The general theory of Sec. 2 is applied to a specific example given by a singularly perturbed, damped, Duffing oscillator with additive, Gaussian noise in Sec. 3. This section contains analytical results and their comparison with numerical computation. The conclusions are contained in Sec. 4.

2. General Theory. We consider the following general $(m + n)$ -dimensional system of stochastic differential equations with two well-separated time scales:

$$(2.1a) \quad \dot{\mathbf{x}} = \mathbf{A}\mathbf{x} + \mathbf{F}(\mathbf{x}, \mathbf{y}, \Phi),$$

$$(2.1b) \quad \epsilon \dot{\mathbf{y}} = \mathbf{B}\mathbf{y} + \mathbf{G}(\mathbf{x}, \mathbf{y}, \Psi),$$

where ϵ is a small parameter, $\mathbf{x}(t) \in \mathbb{R}^m$, $\mathbf{y}(t) \in \mathbb{R}^n$, $\Phi(t)$ and $\Psi(t)$ describe stochastic forces with adjustable intensity, \mathbf{A} and \mathbf{B} are constant matrices, and \mathbf{F} and \mathbf{G} are stochastic, nonlinear functions.

2.1. Deterministic Center Manifold. To begin, we remove the stochastic terms from Eqs. (2.1a) and (2.1b) so that $\mathbf{F} = \mathbf{F}(\mathbf{x}, \mathbf{y})$ and $\mathbf{G} = \mathbf{G}(\mathbf{x}, \mathbf{y})$. Let $t = \epsilon\tau$. Denoting $\dot{}$ as d/dt and $'$ as $d/d\tau$, then the deterministic form of Eqs. (2.1a) and (2.1b) is transformed to the following system of equations:

$$(2.2a) \quad \mathbf{x}' = \epsilon [\mathbf{A}\mathbf{x} + \mathbf{F}(\mathbf{x}, \mathbf{y})],$$

$$(2.2b) \quad \mathbf{y}' = \mathbf{B}\mathbf{y} + \mathbf{G}(\mathbf{x}, \mathbf{y}),$$

$$(2.2c) \quad \epsilon' = 0.$$

To recast the problem in a more general framework, we treat ϵ as a state variable, let $\bar{\mathbf{A}} = \epsilon\mathbf{A}$ and $\bar{\mathbf{F}} = \epsilon\mathbf{F}$, and write Eqs. (2.2a)-(2.2c) as

$$(2.3a) \quad \mathbf{x}' = \bar{\mathbf{A}}\mathbf{x} + \bar{\mathbf{F}}(\mathbf{x}, \mathbf{y}, \epsilon),$$

$$(2.3b) \quad \mathbf{y}' = \mathbf{B}\mathbf{y} + \mathbf{G}(\mathbf{x}, \mathbf{y}),$$

$$(2.3c) \quad \epsilon' = 0.$$

If $\bar{\mathbf{A}}$ and \mathbf{B} are constant matrices such that all of the eigenvalues of $\bar{\mathbf{A}}$ have zero real parts, while all of the eigenvalues of \mathbf{B} have negative real parts, then the system will rapidly collapse onto a lower-dimensional manifold given by center manifold theory [7]. Furthermore, we will consider examples where the solution decays throughout the transient and then stays close to the lower-dimensional manifold.

If the center manifold is given by

$$(2.4) \quad \mathbf{y} = \mathbf{h}(\mathbf{x}, \epsilon),$$

then substitution of Eq. (2.4) into Eq. (2.3b) leads to the following center manifold condition:

$$(2.5) \quad \mathbf{h}_{\mathbf{x}} [\bar{\mathbf{A}}\mathbf{x} + \bar{\mathbf{F}}(\mathbf{x}, \mathbf{h}(\mathbf{x}, \epsilon), \epsilon)] = \mathbf{B}\mathbf{h}(\mathbf{x}, \epsilon) + \mathbf{G}(\mathbf{x}, \mathbf{h}(\mathbf{x}, \epsilon)),$$

where $\mathbf{h}_{\mathbf{x}}$ denotes the partial derivative of \mathbf{h} with respect to \mathbf{x} . Although it is generally not possible to solve Eq. (2.5) for \mathbf{h} , one can approximate the center manifold by expanding \mathbf{h} in the following way:

$$(2.6) \quad \mathbf{h}(\mathbf{x}, \epsilon) = \mathbf{h}_0(\mathbf{x}) + \epsilon\mathbf{h}_1(\mathbf{x}) + \epsilon^2\mathbf{h}_2(\mathbf{x}) + \mathcal{O}(\epsilon^3).$$

Typically, this approximation of $\mathbf{h}(\mathbf{x}, \epsilon)$ is found by substituting Eq. (2.6) into the center manifold condition [Eq. (2.5)] and matching coefficients.

2.2. Optimal Escape Path and Escape Rate. Starting with the center manifold equation given by Eq. (2.6) to a particular order, the dynamics on the center manifold can be found by substitution of Eq. (2.6) into Eq. (2.2a) [using the relation given by Eq. (2.4)]. Therefore, the dynamics are determined by

$$(2.7) \quad \mathbf{x}' = \epsilon [\mathbf{A}\mathbf{x} + \mathbf{F}(\mathbf{x}, \mathbf{h}(\mathbf{x}, \epsilon))] = \epsilon \mathbf{H}(\mathbf{x}, \epsilon),$$

and use of the relation between t and τ leads to the following:

$$(2.8) \quad \dot{\mathbf{x}} = \mathbf{A}\mathbf{x} + \mathbf{F}(\mathbf{x}, \mathbf{h}(\mathbf{x}, \epsilon)) = \mathbf{H}(\mathbf{x}, \epsilon).$$

Equation (2.8) is a deterministic equation. However, now that we have reduced the dimension of the problem, we return to considering a stochastic problem by “naïvely” adding a noise vector to the right-hand side of Eq. (2.8) so that one has

$$(2.9) \quad \dot{\mathbf{x}} = \mathbf{H}(\mathbf{x}, \epsilon) + \sqrt{2D}\mathbf{\Phi}(t),$$

where D is the noise intensity. Each of the noise components, ϕ_i , of $\mathbf{\Phi}$ in Eq. (2.9) describes a stochastic white force that is characterized by the following correlation functions:

$$(2.10a) \quad \langle \phi_i(t) \rangle = 0,$$

$$(2.10b) \quad \langle \phi_i(t)\phi_j(t') \rangle = \delta(t-t')\delta_{ij}.$$

The following analysis to determine the optimal escape path may be performed using Eqs. (2.9)-(2.10b), a system with an arbitrary number of degrees of freedom [18]. However, since we ultimately are interested in applying this general theory to a two-dimensional (2D) surface flow that reduces via the center manifold to a one-dimensional (1D) equation, for simplicity we consider the 1D version of Eq. (2.9) given as

$$(2.11) \quad \dot{x} = H(x, \epsilon) + \sqrt{2D}\phi(t),$$

where $\phi(t)$ is characterized by the correlation functions given by Eqs. (2.10a) and (2.10b).

We assume that $H(x, \epsilon)$ is associated with a potential function $U(x, \epsilon)$, [$H(x, \epsilon) = -dU(x, \epsilon)/dx$] with stable states (attractors) located at $x = x_a$ and an unstable state (saddle) located at $x = x_s$. Then Eq. (2.11) corresponds to a Langevin equation of a particle in an over-damped potential well.

In the absence of noise, a particle located in the potential well will approach the stable, attracting state. However, the noise may organize as an effective force which acts on the particle and “pushes” the particle from the attractor to the saddle located at the top of the potential well barrier. The path along which the particle leaves the basin of attraction due to such an effective noise force is an escape path.

Given that $\phi(t)$ is uncorrelated Gaussian noise, the probability of optimal escape is

$$(2.12) \quad P[x_{\text{esc}}] = C \exp \left(-\frac{1}{2D} \int_{-\infty}^{\infty} \phi_{\text{opt}}^2 dt \right) = C \exp(-R/D),$$

where

$$(2.13) \quad R = \frac{1}{2} \int_{-\infty}^{\infty} \phi_{\text{opt}}^2 dt = \frac{1}{2} \int_{-\infty}^{\infty} L(x, \dot{x}; t) dt,$$

and ϕ_{opt} denotes the stochastic fluctuations corresponding to the trajectory that moves along the optimal escape path. In Eq. (2.12), C is a pre-factor that depends on the noise intensity. In order to maximize the probability of escape, one must minimize the exponent given by Eq. (2.13). Using the Euler-Lagrange equation of motion, it is now possible to solve for the optimal escape path.

It also is possible to derive an expression for the escape rate from an attractor to the saddle, which is located at the top of the potential well barrier. In general, if the stochastic trajectory of a particle is given by

$$(2.14) \quad \dot{x} = -\frac{dU(x, \epsilon)}{dx} + \sqrt{2D}\phi(t),$$

with $U(x, \epsilon)$ some potential (as we have assumed), then for Gaussian noise, the escape rate from the attractor (located at $x = x_a$) to the unstable saddle (located at $x = x_s$ at the top of the barrier) is given by

$$(2.15) \quad W(D) = \frac{\sqrt{|Q(x_s, \epsilon)|Q(x_a, \epsilon)}}{2\pi} \exp(-\Delta U/D),$$

where $Q(x, \epsilon) = d^2U(x, \epsilon)/dx^2$ and ΔU is the activation energy of escape (depth of the potential well) [25].

If $W(D)$ is the escape rate, then $1/W(D)$ gives the mean escape time, and the natural log of the mean escape time is therefore

$$(2.16) \quad \log\left(\frac{1}{W(D)}\right) = \log\left(\frac{2\pi}{\sqrt{|Q(x_s, \epsilon)|Q(x_a, \epsilon)}}\right) + \frac{\Delta U}{D}.$$

It should be noted that to ensure the particle escapes from the potential well, one could compute the escape rate (and the mean escape time) from the attractor to a point located somewhere in the second potential well (i.e. the particle escapes from the first basin of attraction if it climbs out of the potential well to the saddle located at the top of the potential well barrier and then continues past the saddle to some point located in the second basin of attraction). However, this movement of the point at which one claims the particle has escaped from the potential well will create a change in the pre-factor of Eq. (2.15) along with a corresponding change in the first term on the right-hand side of Eq. (2.16) [25].

As we have previously noted, we consider systems whose solution decays exponentially throughout the transient and then stays close to the lower-dimensional center manifold. There are no secular terms in the asymptotic expansion since we are not looking at periodic orbits, and the result is valid for all time. Moreover, any noise drift on the center manifold will result in bounded solutions due to sufficient dissipation transverse to the manifold. This behavior is in direct contrast to the finite-time solutions on manifolds of relaxation-type oscillators whereby the time scale of escape must be shorter than the lifetime of the trajectories on the manifold [10, 22]. This lifetime issue does not pertain to the systems we consider since there will be no oscillations.

2.3. Stochastic Center Manifold and the Normal Form Coordinate Transform. In a manner similar to that shown in Sec. 2.1, the stochastic system given by Eqs. (2.1a) and (2.1b) can be transformed [3] to the form given by Eqs. (2.3a)-(2.3c), where now $\bar{\mathbf{F}} = \bar{\mathbf{F}}(\mathbf{x}, \mathbf{y}, \epsilon, \Phi)$ and $\mathbf{G} = \mathbf{G}(\mathbf{x}, \mathbf{y}, \Psi)$. If $\bar{\mathbf{A}}$ and \mathbf{B} satisfy the same spectral conditions as for the deterministic system, and if the stochastic time dependence found in $\bar{\mathbf{F}}$ and \mathbf{G} is due to independent white noise processes, then there exists a stochastic center manifold for the original stochastic system [6].

One method for computing the stochastic center manifold for systems with both fast and slow dynamics uses the construction of a normal form coordinate transform that not only reduces the dimension of the dynamics, but also separates all of the fast processes from all of the slow processes [42]. While this type of normal form coordinate transform may be used to find deterministic center manifolds, the application of this transform to stochastic systems is particularly interesting since white noise has fluctuations on all scales.

There are many publications, such as [34, 9, 40, 41] which deal with the simplification of a stochastic dynamical system using a stochastic normal form transformation. In these articles, the noise term is multiplied by a small parameter, and therefore, the resulting stochastic normal form is a perturbation of the deterministic normal form. Furthermore, one can find in [9, 41] normal form transformations that involve anticipative noise processes. However, these integrals of the noise process into the future were not dealt with rigorously in [9, 41].

Rigorous, theoretical analysis to support normal form coordinate transforms (and center manifold reduction) was developed in [2, 1]. In this work, the technical problem of the anticipative noise integrals also was dealt with rigorously. Later, another stochastic normal form transformation was developed [42]. This new method is such that “anticipation can ... always [be] removed from the slow modes with the result that no anticipation is required after the fast transients decay” (Ref. [42], pp. 13). An advantage of removing anticipation is the simplification of the normal form. Nonetheless, this simpler normal form retains its accuracy with the original stochastic system. Furthermore, when modeling the macroscopic behavior of microscopic, stochastic systems, it is desirable to avoid anticipation in the normal form [42].

It is important to note that the normal form is valid for all time since it is just a coordinate transform. Furthermore, the dynamics also are valid for all time as long as the truncation error is small enough for the problem of interest.

In the example of Sec. 3, we shall use the method of [42] to simplify our stochastic dynamical system to one that emulates the long-term dynamics of the original, multiple-time-scale system. The method involves five principles, which we recapitulate here for the purpose of clarity. The principles are as follows:

1. Avoid unbounded, secular terms in both the transformation and the evolution equations to ensure a uniform asymptotic approximation.
2. Decouple all of the slow processes from the fast processes to ensure a valid long-term model.
3. Insist that the stochastic slow manifold is precisely the transformed fast processes coordinate being equal to zero.
4. To simplify matters, eliminate as many as possible of the terms in the evolution equations.
5. Try to remove all fast processes from the slow processes by avoiding as much as possible the fast time memory integrals in the evolution equations.

In practice, the original stochastic system of equations (which satisfy the necessary

spectral requirements) in (\mathbf{x}, \mathbf{y}) coordinates is transformed to a new (\mathbf{X}, \mathbf{Y}) coordinate system using a stochastic coordinate transform as follows:

$$(2.17a) \quad \mathbf{x} = \mathbf{X} + \boldsymbol{\xi}(\mathbf{X}, \mathbf{Y}, t),$$

$$(2.17b) \quad \mathbf{y} = \mathbf{Y} + \boldsymbol{\eta}(\mathbf{X}, \mathbf{Y}, t),$$

where the specific form of Eqs. (2.17a) and (2.17b) is chosen to simplify the original system according to the five principles listed previously. The terms $\boldsymbol{\xi}(\mathbf{X}, \mathbf{Y}, t)$ and $\boldsymbol{\eta}(\mathbf{X}, \mathbf{Y}, t)$ are found using an iterative procedure that will be demonstrated using the singularly perturbed, damped, stochastic Duffing oscillator model in Sec. 3. Theoretical details can be found in [42].

3. Example - Singularly Perturbed Stochastic Duffing Oscillator. We consider the following singularly perturbed, damped, Duffing oscillator system with additive noise:

$$(3.1a) \quad \dot{x} = y + \sqrt{2D}\phi(t),$$

$$(3.1b) \quad \epsilon \dot{y} = (x - x^3 - y),$$

where D is the noise intensity and $\phi(t)$ describes a stochastic white force that is characterized by the correlation functions given in Eqs. (2.10a) and (2.10b).

In this example, the noise is added only to the x equation. Additionally, one could consider two other scenarios. In the first scenario, noise is added to both the x and y equations, while in the second scenario, noise is added only to the y equation. To implement the first scenario, one adds $\sqrt{2D}\phi_1(t)$ to the right-hand side of the x equation and $\sqrt{2D}\phi_2(t)$ to the right-hand side of the y equation [where $\phi_1(t)$ and $\phi_2(t)$ describe stochastic white forces of intensity D that are characterized by the correlation functions given in Eqs. (2.10a) and (2.10b)]. To implement the second scenario, noise is added only to the y equation. However, unlike the example [Eqs. (3.1a) and (3.1b)] and the first scenario, in this case the noise term must be scaled by $\sqrt{\epsilon}$ and the potential function must be scaled by ϵ [44]. Although the following results pertain to Eqs. (3.1a) and (3.1b), we have checked that one obtains similar results for the other two scenarios.

The system given by Eqs. (3.1a) and (3.1b) is very strongly damped when $\epsilon \ll 1$. For the case of an under-damped system, one should consider the dynamics in the limit of weak damping [17].

3.1. Deterministic Center Manifold. Following the general theory of Sec. 2.1, we consider the deterministic form of Eqs. (3.1a) and (3.1b) by setting $\phi(t) = 0$. The slow manifold is found by setting $\epsilon = 0$ in Eq. (3.1b). Solving for y gives the equation of the slow manifold as $y = x - x^3$ [which corresponds to $h_0(x)$ in Eq. (2.6)]. Substitution of this into the deterministic form of Eq. (3.1a) gives the dynamics along the slow manifold as $\dot{x} = x - x^3$.

If, as in Sec. 2.1, we let $t = \epsilon\tau$ and denote $\dot{}$ as d/dt and $'$ as $d/d\tau$, then Eqs. (3.1a) and (3.1b) (with $\phi(t) = 0$) are transformed to the following system:

$$(3.2a) \quad x' = \epsilon y,$$

$$(3.2b) \quad y' = x - x^3 - y,$$

$$(3.2c) \quad \epsilon' = 0.$$

Rearrangement of Eqs. (3.2a)-(3.2c) leads to a system described by constant matrices $\bar{\mathbf{A}}$ and \mathbf{B} that satisfy the spectral requirements of Sec. 2.1. Furthermore, since the x and ϵ variables are associated with the $\bar{\mathbf{A}}$ matrix (eigenvalues with zero real parts), and the y variable is associated with the \mathbf{B} matrix (eigenvalues with negative real parts), we know that the center manifold is given by $y = h(x, \epsilon)$.

The center manifold condition is given by Eq. (2.5), and we approximate the center manifold [Eq. (2.6)] as follows:

$$(3.3a) \quad h(x, \epsilon) = h_0(x) + \epsilon h_1(x) + \epsilon^2 h_2(x) + \mathcal{O}(\epsilon^3)$$

$$(3.3b) \quad \begin{aligned} &= c_0 + c_{01}\epsilon + c_{10}x + c_{02}\epsilon^2 + c_{11}x\epsilon + c_{20}x^2 \\ &+ c_{03}\epsilon^3 + c_{12}x\epsilon^2 + c_{21}x^2\epsilon + c_{30}x^3 + \mathcal{O}(\gamma^4), \end{aligned}$$

where $c_0, c_{01}, c_{10}, c_{02}, \dots$ are unknown coefficients, and $\gamma = |(x, \epsilon)|$ so that γ provides a count of the number of x and ϵ factors in any one term. The center manifold condition for this example is given by

$$(3.4) \quad \frac{\partial h(x, \epsilon)}{\partial x} [\epsilon h(x, \epsilon)] = -h(x, \epsilon) + x - x^3.$$

By substituting Eq. (3.3b) into Eq. (3.4) and matching the different orders to find the coefficients, one finds the following center manifold equation (expanded to sixth-order):

$$(3.5a) \quad \begin{aligned} h(x, \epsilon) &= x - \epsilon x + 2\epsilon^2 x - x^3 - 5\epsilon^3 x + 4\epsilon x^3 + 14\epsilon^4 x \\ &- 20\epsilon^2 x^3 - 42\epsilon^5 x + 104\epsilon^3 x^3 - 3\epsilon x^5 + \mathcal{O}(\gamma^7) \end{aligned}$$

$$(3.5b) \quad \begin{aligned} &= x - x^3 + \epsilon(-x + 4x^3 - 3x^5) + \epsilon^2(2x - 20x^3) \\ &+ \epsilon^3(-5x + 104x^3) + \epsilon^4(14x) + \epsilon^5(-42x) + \mathcal{O}(\gamma^7). \end{aligned}$$

Note that by letting $\epsilon = 0$, one recovers the zero-order approximation, $h_0(x)$ (the slow manifold). In addition, since ϵ is now a state variable, the first nontrivial correction term to the zero-order approximation is a quadratic term.

3.2. Optimal Escape Path and Escape Rate. Consider the third-order center manifold equation given by $h(x, \epsilon) = x - x^3 - \epsilon x + 2\epsilon^2 x$ [see Eq. (3.5a)]. Following Sec. 2.2, the dynamics on the center manifold are given by $x' = \epsilon h(x, \epsilon)$ [see Eq. (2.7)]. Use of the relation $t = \epsilon \tau$ leads to the following deterministic equation:

$$(3.6) \quad \dot{x} = h(x, \epsilon) = x - x^3 - \epsilon x + 2\epsilon^2 x.$$

We “naïvely” add the noise term $\phi(t)$ to the right-hand side of Eq. (3.6) as in Eqs. (2.9) and (2.11) so that

$$(3.7) \quad \dot{x} = x - x^3 - \epsilon x + 2\epsilon^2 x + \sqrt{2D}\phi(t).$$

Equation (3.7) corresponds to a Langevin equation of a particle in an overdamped quartic potential well with stable states (attractors) located at $x = x_a = \pm\sqrt{1 - \epsilon + 2\epsilon^2}$ and an unstable state (saddle) located at $x = x_s = 0$.

The probability of optimal escape is given by Eqs. (2.12) and (2.13). Solution of the Euler-Lagrange equation of motion leads to the following optimal escape path:

$$(3.8) \quad x_{\text{esc}} = \sqrt{\frac{A}{1 + 3 \exp(2At)}},$$

where $A = 1 - \epsilon + 2\epsilon^2$. Note that $x_{\text{esc}} \rightarrow \sqrt{A}$ as $t \rightarrow -\infty$ while $x_{\text{esc}} \rightarrow 0$ as $t \rightarrow \infty$. This path is a heteroclinic orbit from the basin of attraction located at $x = \sqrt{A}$ to the saddle located at $x = 0$.

Using Eq. (3.8) along with

$$(3.9) \quad \dot{x}_{\text{esc}} = x_{\text{esc}} - x_{\text{esc}}^3 - \epsilon x_{\text{esc}} + 2\epsilon^2 x_{\text{esc}} + \sqrt{2D} \phi_{\text{opt}}(t),$$

we find that the optimal noise is given by the following:

$$(3.10) \quad \phi_{\text{opt}}(t) = \frac{1}{\sqrt{2D}} \times \sqrt{\frac{A}{1 + 3 \exp(2At)}} \times \left[\frac{-6A \exp(2At)}{1 + 3 \exp(2At)} \right].$$

Since A is a function of ϵ , the shape of $\phi_{\text{opt}}(t)$ will be affected by the value of ϵ . With $D = 0.05$, Fig. 5.1(a) shows $\phi_{\text{opt}}(t)$ for various values of ϵ . To obtain a clearer view, Fig. 5.1(b) shows a section of Fig. 5.1(a). One can see in Figs. 5.1(a) and 5.1(b) that ϵ has an effect on both the pulse width and amplitude. Starting with $\epsilon = 0.02$, the pulse amplitude decreases monotonically and the pulse width increases monotonically as ϵ increases to $\epsilon = 0.25$ (the value of ϵ for which A is minimized). As ϵ continues to increase beyond $\epsilon = 0.25$, the pulse amplitude increases monotonically and the pulse width decreases monotonically.

Using the theory outlined in Sec. 2.2, we now derive an expression for the escape rate from one of the attractors to the saddle in order to predict the change in escape rate caused by varying the value of ϵ and D .

Since the stochastic (“naïve”), third-order center manifold dynamical equation given by Eq. (3.7) has the form of Eq. (2.14), then the escape rate from the attractor located at $x = x_a = \sqrt{1 - \epsilon + 2\epsilon^2}$ to the saddle located at $x = x_s = 0$ can be found using Eq. (2.15). The escape rate is given as follows:

$$(3.11a) \quad W(\epsilon, D) = \frac{\sqrt{|-1 + \epsilon - 2\epsilon^2|(2 - 2\epsilon + 4\epsilon^2)}}{2\pi} \times \exp(-\Delta U/D),$$

$$(3.11b) \quad \Delta U = \left| \frac{-1 + 2\epsilon - 5\epsilon^2 + 4\epsilon^3 - 4\epsilon^4}{4} \right|.$$

Appendix A contains similar expressions for the escape rate that are found using the fourth-order and fifth-order stochastic (“naïve”) center manifold dynamical equations.

3.3. Stochastic Center Manifold and the Normal Form Coordinate Transform. To more accurately describe the stochastic effects, we will derive the normal form coordinate transform (and thus the stochastic center manifold) for the singularly perturbed, stochastic Duffing system given by Eqs. (3.1a) and (3.1b). As demonstrated previously, use of the $t = \epsilon\tau$ transformation leads to the following system:

$$(3.12a) \quad x' = \epsilon(y + \sqrt{2D}\phi) = \epsilon(y + \sigma\phi),$$

$$(3.12b) \quad y' = x - x^3 - y,$$

$$(3.12c) \quad \epsilon' = 0,$$

where σ is the standard deviation of the noise intensity $D = \sigma^2/2$.

The construction of the normal form is quite tedious and complicated. However, the result allows one to determine if there are any noise terms that cause a significant difference between the average stochastic center manifold (the stochastic center manifold generally fluctuates about an average location) and the deterministic center manifold.

For this problem, it turns out that the noise terms that could lead to a difference between the deterministic and average stochastic center manifolds occur at very high order in the normal form expansion. Therefore, the correction to the deterministic center manifold is minimal, and we expect that the deterministic results of Sec. 3.1 and Sec. 3.2 will agree very well with numerical computations using the original stochastic system [Eqs. (3.1a) and (3.1b)].

We proceed by showing how to use the method of [42] described in Sec. 2.3 to construct a normal form coordinate transform that separates the slow and fast dynamics of Eqs. (3.12a) and (3.12b). In what follows, we outline the steps involved in the first iteration, while details regarding the higher iterations are provided in the appendices.

3.3.1. First Iteration. We begin by letting

$$(3.13a) \quad x \approx X,$$

$$(3.13b) \quad X' \approx 0,$$

and by finding a change to the y coordinate (fast process) with the form

$$(3.14a) \quad y = Y + \eta(\tau, X, Y) + \dots,$$

$$(3.14b) \quad Y' = -Y + G(\tau, X, Y) + \dots,$$

where η and G are small corrections to the coordinate transform and the corresponding evolution equation. Substitution of Eqs. (3.13a)-(3.14b) into Eq. (3.12b) gives the following equation:

$$(3.15) \quad Y' + \frac{\partial \eta}{\partial \tau} + \frac{\partial \eta}{\partial X} \frac{\partial X}{\partial \tau} + \frac{\partial \eta}{\partial Y} \frac{\partial Y}{\partial \tau} = -Y - \eta + X - X^3.$$

Replacing $Y' = \partial Y / \partial \tau$ with $-Y + G$ [Eq. (3.14b)], noting that $\partial X / \partial \tau = 0$ [Eq. (3.13b)], and ignoring the term $\partial \eta / \partial Y \cdot G$ since it is a product of small corrections leads to the following:

$$(3.16) \quad G + \frac{\partial \eta}{\partial \tau} - Y \frac{\partial \eta}{\partial Y} + \eta = X - X^3.$$

Equation (3.16) must now be solved for G and η . In order to keep the evolution equation [Eq. (3.14b)] as simple as possible (principle (4) of Sec. 2.3), we let $G = 0$, which means that the coordinate transform [Eq. (3.14a)] is modified by $\eta = X - X^3$. Therefore, the new approximation of the coordinate transform and its dynamics are given by

$$(3.17a) \quad y = Y + X - X^3 + \mathcal{O}(\zeta^2),$$

$$(3.17b) \quad Y' = -Y + \mathcal{O}(\zeta^2),$$

where $\zeta = |(X, Y, \epsilon, \sigma)|$ so that ζ provides a count of the number of X , Y , ϵ , and σ factors in any one term.

3.3.2. Higher Iterations. The construction of the normal form continues by seeking corrections, ξ and F , to the x coordinate transform and the X evolution using the updated residual of the x equation [Eq. (3.12a)], and by seeking corrections, η and G , to the y coordinate transform and the Y evolution equation using the updated residual of the y equation [Eq. (3.12b)]. Details regarding the second iteration can be found in Appendix B.

The derivation of ξ and F in the second and fourth iterations along with the derivation of η and G in the third iteration leads to the following updated approximation of the coordinate transforms and their corresponding evolution equations:

$$(3.18a) \quad \begin{aligned} y = & Y + X - X^3 + \epsilon(-X + 4X^3 - 3X^5) \\ & + \epsilon\sigma(-e^{-\tau} * \phi + 3X^2e^{-\tau} * \phi) + 3\epsilon^2XY^2 + \mathcal{O}(\zeta^3), \end{aligned}$$

$$(3.18b) \quad Y' = -Y + \epsilon(-Y + 3X^2Y) + \mathcal{O}(\zeta^3),$$

$$(3.19a) \quad \begin{aligned} x = & X - \epsilon Y + \epsilon^2(Y - 3X^2Y) \\ & + \epsilon^2\sigma(e^{-\tau} * \phi - 3X^2e^{-\tau} * \phi) + \mathcal{O}(\zeta^4), \end{aligned}$$

$$(3.19b) \quad \begin{aligned} X' = & \epsilon(X - X^3) + \epsilon\sigma\phi + \epsilon^2(-X + 4X^3 - 3X^5) \\ & + \epsilon^2\sigma(-\phi + 3X^2\phi) + \mathcal{O}(\zeta^4), \end{aligned}$$

where

$$(3.20) \quad e^{-\tau} * \phi = \int_{-\infty}^{\tau} \exp[-(\tau - s)]\phi(s) ds.$$

Details regarding the derivation of Eqs. (3.18a) and (3.18b) can be found in Appendix C, while details of the derivation of Eqs. (3.19a) and (3.19b) can be found in Appendix D.

One can continue this iterative procedure to obtain higher order terms in the expansions of the coordinate transform and normal form. For the stochastic Duffing system under consideration, the fifth and sixth iterations lead to updated approximations of the x and y coordinate transforms (along with their associated evolution

equations) that are extremely long and complicated. These approximations can be found in Appendix E.

In the higher order transform given by Eqs. (E.1a)-(E.1d), one can see the appearance of quadratic noise terms. For example, one can see terms of the form $e^{-\tau} * (e^{-\tau} * \phi)^2$ in the coordinate transforms [Eqs. (E.1a) and (E.1c)], and one can see terms of the form $\phi e^{-\tau} * \phi$ in one of the evolution equations [Eq. (E.1d)]. This quadratic noise is important because it leads to the creation of a deterministic drift within the slow dynamics [42, 41]. Furthermore, the stochastic center manifold generally undergoes fluctuations about a mean or average location. This average stochastic center manifold is usually different from the deterministic center manifold, and it is the quadratic noise process that generates this difference.

3.3.3. Comparison with Deterministic Center Manifold and Effect of Quadratic Noise. Letting $Y = 0$ and $\sigma = 0$ in Eqs. (E.1a) and (E.1c) leads to the following deterministic center manifold equation:

$$(3.21a) \quad x = X,$$

$$(3.21b) \quad y = X - X^3 + \epsilon(-X + 4x^3 - 3X^5) + \epsilon^2(2X - 20X^3 + 42X^5) + \epsilon^3(-X + 16X^3 - 66X^5 + 96X^7 - 45X^9) + \mathcal{O}(\epsilon^3).$$

Comparison of Eqs. (3.21a) and (3.21b) with Eq. (3.5b) shows agreement through the $\mathcal{O}(\epsilon^2)$ terms. There appears to be a discrepancy at order $\mathcal{O}(\epsilon^3)$. However, we have checked that this apparent discrepancy is resolved by expanding the stochastic normal form coordinate transform to even higher order. For example, the seventh iteration will yield a $-4\epsilon^3 X$ term in the y coordinate transform. When added to the existing $-\epsilon^3 X$ term, there is an agreement with the $-5\epsilon^3 x$ term in Eq. (3.5b).

Letting $Y = 0$ in Eqs. (E.1a) and (E.1c) leads to the stochastic center manifold equation. If one takes the expectation of this stochastic center manifold equation and uses the following identities [42]:

$$(3.22) \quad E[e^{\pm\tau} * \phi] = e^{\pm\tau} * E[\phi],$$

$$(3.23) \quad E[(e^{\pm\tau} * \phi)^2] = \frac{1}{2},$$

then one obtains the following:

$$(3.24) \quad E[y] = X - X^3 + \epsilon(-X + 4X^3 - 3X^5) + \epsilon^2(2X - 20X^3 + 42X^5) + \epsilon^3(-X + 16X^3 - 66X^5 + 96X^7 - 45X^9) + \epsilon^4\sigma^2(-3X/2 + 9X^3 - 27X^5/2),$$

where the $\mathcal{O}(\epsilon^4\sigma^2)$ terms are associated with the quadratic noise terms in Eq. (E.1a).

The average stochastic center manifold equation given by Eq. (3.24) can now be used in conjunction with the theory outlined in Sec. 2.2 to find an analytical expression for the escape rate. This calculation has been performed, but because the noise effects occur at such high order [$\mathcal{O}(\epsilon^4\sigma^2)$], the correction to the stochastic (“naïve”) result is minimal.

3.4. Numerical Computation of Escape Time. When $\sigma = 0$ (no noise), the original, singularly perturbed problem given by Eqs. (3.1a) and (3.1b), has three equilibrium points given by $(-1, 0)$, $(0, 0)$, and $(1, 0)$. At the initial time, $t = 0$, a particle is randomly placed near the stable, attracting point $(1, 0)$ within a circle of radius 0.1 centered at $(1, 0)$.

Equations (3.1a) and (3.1b) are numerically integrated using a stochastic fourth-order Runge-Kutta scheme [43, 29] with a constant time step size, δt , that depends on the value of ϵ ($\delta t = 0.01$ for $\epsilon < 0.1$, while $\delta t = 0.1$ for $\epsilon \geq 0.1$), and the time needed for the particle to escape from the basin of attraction is determined. This escape time is based on either the time it takes the particle to cross the $x < -0.2$ barrier, which means the particle has escaped across the unstable saddle, and has entered the second basin of attraction with stable, attracting point $(-1, 0)$, or when the maximum time (10,000,000 for $\delta t = 0.01$ and 100,000,000 for $\delta t = 0.1$) has been reached.

This computation was performed for 10,000 particles, and the mean escape time was determined. In these computations, ϵ ranged from $\epsilon = 0.02$ to $\epsilon = 1.5$, and σ ranged from $\sigma = 0.26$ to $\sigma = 0.5$. Figure 5.2 shows a contour plot of the natural log of the mean escape time plotted for the above range of ϵ and $1/D = 2/\sigma^2$ values.

By taking a vertical slice of Fig. 5.2, one can look at a plot of the natural log of the mean escape time versus $1/D$ for a fixed value of ϵ . Figure 5.3(a) shows a vertical slice of Fig. 5.2 taken at $\epsilon = 0.1$ along with a line of best fit through these numerically computed data points. The slope of the best fit line is $m = 0.2505$. From Eq. (2.16), we see that if one plots the natural log of the mean escape time vs. $1/D$, then the theoretical slope of this line is given by ΔU , the depth of the potential well. If $\epsilon = 0$, the depth of the potential well corresponding to Eqs. (3.1a) and (3.1b) is $\Delta U = 0.25$, which compares very well with the numerical result for $\epsilon = 0.1$.

Figure 5.3(b) shows several vertical slices of Fig. 5.2 taken at various values of ϵ . As in Fig. 5.3(a), there is a line of best fit through the data points corresponding to each choice of ϵ .

Numerical computations have been performed for values of ϵ as small as 0.02. The slopes of the lines of best fit through the data for these small values of ϵ are very close to 0.25. The data and their lines of best fit are not shown in Fig. 5.3(b) since the plots would obscure one another (and they would all be obscured by the $\epsilon = 0.1$ plot).

One can see in Fig. 5.3(b) that as the value of ϵ increases (which means that the system moves further and further away from the over-damped regime), the slope of the line of best fit decreases. The slope values are as follows: for $\epsilon = 0.2$, $m = 0.2466$; for $\epsilon = 0.3$, $m = 0.2398$; for $\epsilon = 0.4$, $m = 0.2287$; for $\epsilon = 0.5$, $m = 0.2165$; and for $\epsilon = 1.0$, $m = 0.1549$. When the system is in an under-damped regime, the slope of the best fit line no longer agrees with the theoretical value when $\epsilon = 0$ ($m = 0.25$). However, there still is a nice scaling behavior. One should note that in general the escape rate computed using the one-dimensional system found by letting $\epsilon = 0$ may be different than the escape rate of the associated two-dimensional system with $\epsilon \rightarrow 0$ [11]. A specific example may be found in the case of extinction processes [46], where the rate to extinction has no limit when a singular parameter becomes small.

As shown in Sec. 2.2, Eqs. (3.11a) and (3.11b) can be used to find analytical values of the natural log of the mean escape time. By varying the value of D and by fixing the value of ϵ , we can compare the analytical mean escape time found using Eqs. (3.11a) and (3.11b) [or Eqs. (A.2a)-(A.2d); Eqs. (A.4a)-(A.4d)] with the numerically computed mean escape time shown in Figs. 5.2 and 5.3.

With $\epsilon = 0.02$, Fig. 5.4(a) shows a comparison between the numerically computed mean escape time (Fig. 5.2) and the analytically computed mean escape time found using the fifth-order center manifold equation [Eqs. (A.4a)-(A.4d)]. Figure 5.4(a) also contains lines of best fit passing through the data points associated with numerical and analytical computation.

One can see from Fig. 5.4(a) that there is good agreement between the two methods. The slope of the line of best fit through the numerical data is $m_{\text{num}} = 0.2536$, while the slope of the line of best fit through the analytical data is $m_{\text{ana}} = \Delta U = 0.2591$. One also can see in Fig. 5.4(a) that there is a slight discrepancy between the analytical and numerical y -intercept values. This is due to the fact that in the numerical computation, the escape time was based on the time for the particle to cross the barrier and descend partially into the second basin of attraction, while the analytical escape time was based on the time for the particle to reach the top of the barrier.

The two methods continue to agree well as ϵ is increased to $\epsilon = 0.1$ [Fig. 5.4(b)] and $\epsilon = 0.14$ [Fig. 5.4(c)]. Beyond $\epsilon = 0.14$, the analytical result begins to diverge from the numerical result, and this divergence increases as ϵ increases. An example of this divergence is shown for $\epsilon = 0.2$ in Fig. 5.4(d). The slopes of the lines of best fit are as follows: for $\epsilon = 0.1$, $m_{\text{num}} = 0.2505$ and $m_{\text{ana}} = \Delta U = 0.2624$; for $\epsilon = 0.14$, $m_{\text{num}} = 0.2490$ and $m_{\text{ana}} = \Delta U = 0.2385$; and for $\epsilon = 0.2$, $m_{\text{num}} = 0.2466$ and $m_{\text{ana}} = \Delta U = 0.1859$. Note that by linearizing the deterministic form of Eqs. (3.1a)-(3.1b) about the stable, attracting point $(1, 0)$, one finds that the critical damping value is $\epsilon_{\text{cr}} = 0.125$. This value agrees well with the value at which the good comparison between the analytical result and numerical result begins to break down.

As stated in Sec. 3.3, we have computed the analytical escape rate of the particle using the stochastic center manifold. Again, the stochastic correction is minimal, and therefore these analytical mean escape times are very close in value to those found using the “naïve” approach. We do not show figures comparing this analytical result with the numerical result since there is no noticeable difference from the plots shown in Figs. 5.4(a)-5.4(d).

3.5. Numerical Computation of Escape Prehistory. For each of the 10,000 particles that were initially placed in one of the attracting basins and which later escaped from this basin, across the saddle, and into the other basin of attraction, we retain $t = 200$ worth of the particle’s path prior to escape. By creating a histogram representing the probability density, p_h , of this escape prehistory [14], one can see which regions of the phase space are associated with a high or low probability of particle escape.

An example of a histogram of escape path prehistory is shown in Fig. 5.5(a) for $\epsilon = 0.1$ and $\sigma = 0.3$ (so that $D = \sigma^2/2 = 0.045$). The color-bar values of Fig. 5.5(a) have been normalized by 10^5 . The threshold 0 value in Fig. 5.5(a) is actually about 9000. Therefore, any histogram box containing less than 9000 events shows up as white on the histogram. Figure 5.5(b) is the same as Fig. 5.5(a), but with adjusted color-bar values. Doing this enables one to obtain a clearer view of the escape path prehistory along the separatrix and near the saddle. Figure 5.5(b) also includes the escape path prehistory for one particular particle. To avoid clutter, we have overlaid only $t = 50$ of path prehistory for this one particle.

Figure 5.6(a) shows Fig. 5.5(a) overlaid with the graph of the slow manifold equation, $y = x - x^3$. Even though this equation is found by setting $\epsilon = 0$ in the deterministic version of Eqs. (3.1a) and (3.1b), we see in Fig. 5.6(a) that the slow

manifold lies very close to the region associated with the highest probability of escape.

Similarly, Fig. 5.6(b) shows Fig. 5.5(a) overlaid with the graphs of the third-order, fourth-order, and fifth-order center manifold equations. Each of these equations may be found by including terms of the appropriate order from Eq. (3.5a). As in Fig. 5.5(a), the color-bar values of Figs. 5.6(a) and 5.6(b) have been normalized by 10^5 .

One can see from Fig. 5.6(b) that the third-order and fourth-order center manifolds essentially bound the entire region of escape path prehistory, while the fifth-order manifold lies along the region of highest probability of escape. Although it is not shown, it should be noted that the optimal escape path [Eq. (3.8)] associated with the third-order center manifold is a heteroclinic orbit from $x = \sqrt{1 - \epsilon + 2\epsilon^2}$ to $x = 0$ that lies directly on top of a section of the third-order center manifold [solid, green line in Fig. 5.6(b)]. Similarly, the optimal escape paths associated with higher order center manifolds lie directly on top of a section of the corresponding center manifold.

Additionally, one could overlay the histogram of escape path prehistory with the average stochastic center manifold given by Eq. (3.24). However, since the stochastic correction appears at order $\mathcal{O}(\epsilon^4\sigma^2)$, there is no noticeable difference from the manifolds shown in Figs. 5.6(a) and 5.6(b). Therefore, plots of the average stochastic manifold are not shown.

4. Conclusions. A general procedure consisting of elements taken from deterministic and stochastic manifold theory and large fluctuation theory is developed and used to understand the underlying structure of a stochastic dynamical system with two well-separated time scales.

As a first step towards this goal, we have applied the procedure to a generic 2D, singularly perturbed, damped, Duffing oscillator system with additive, Gaussian noise. The deterministic center manifold equation is found by neglecting the stochastic terms. By “naïvely” adding a noise term to the equation that describes the dynamics on the center manifold, the path integral formalism of large fluctuation theory can be used to analytically compute the optimal escape path of the particle from one basin of attraction to another basin of attraction as well as the particle’s escape rate. Comparison of the analytical result with numerical computations shows excellent agreement if the system is in the over-damped regime. There is a shift due to the pre-factor of the distribution, but the exponent is quite accurate. While it is possible to correctly determine the pre-factor using spectral methods, the technique works only for 1D problems [38]. When the system enters the under-damped regime, we must consider the 2D topology rather than the 1D manifold topology that is associated with the over-damped regime [17]. We are currently performing the analysis associated with the under-damped regime, and this will be presented elsewhere.

Additionally, we used numerical computation to create a histogram of the escape path prehistory distribution. The histogram enables one to see regions of the phase space that are associated with high and low probability of particle escape from the basin of attraction. By overlaying the histogram with the deterministic slow manifold, we see that this manifold lies close to the region associated with the highest probability of escape. By comparing the histogram with deterministic center manifolds of various orders, we see that the third-order and fourth-order center manifolds essentially bound the entire region of escape, while the fifth-order center manifold lies very close to the region associated with the highest probability of escape. Therefore one can use these manifolds to accurately describe the location of escape regions. The example considered here is that of a quartic potential which is a generic potential for a pitchfork bifurcation. Therefore, for systems whose center manifolds yield pitchfork dynamics,

we expect similar results to hold when additive noise is considered.

Knowledge of the location of the regions of high and low probability of escape (whether from numerical or analytical results) is extremely useful if one wishes to optimize the amount of time spent in a particular region of phase space. For example, one might wish to keep an autonomous glider in some basin of attraction. Instead of constantly actuating the glider controls to keep the glider stationed at a particular location, one can station the glider initially in a region of low probability of escape. Then, if the glider enters a region of high probability of escape, one actuates the controls to move the glider back to a region with low probability of escape and the controls are switched off. This is similar to the stochastic control used in [45, 13].

As an example, consider a particle whose dynamics are described by Eqs. (3.1a) and (3.1b). Figure 5.7(a) shows the location of the particle (x coordinate) as a function of time t . One can see in Fig. 5.7(a) that the particle moves around the basin of attraction until eventually the stochastic effects cause the particle to escape from the basin at $t \approx 1290$.

By implementing a simple control that pushes the particle into a region of phase space that has a low probability of escape whenever the particle enters a region of high probability of escape, it is possible to keep the particle in the basin of attraction for a much longer amount of time. Figure 5.7(b) shows the location of the particle (x coordinate) as a function of time t with the application of control. One can see in Fig. 5.7(b) that control allows one to keep the particle in the basin of attraction until $t = 10,000$, when the simulation was stopped. Preliminary results show that the application of control increases the mean time to escape from the basin and decreases the total number of particles which escape in a given period of time. A complete analysis of the application of control will appear elsewhere.

Even though we showed that analytical results using a “naïve” approach agree very well with the numerical results in the over-damped regime, to more accurately describe the stochastic effects, we derived the normal form coordinate transform. The normal form enabled us to find the stochastic center manifold. However, the stochastic effects appeared in the manifold equation at high order, so this correction has a minimal effect. Therefore, for this problem at least, one can use the simpler and much less time consuming “naïve” approach.

It should be noted that there are systems where one should not rely on the “naïve” approach. For example, in a Susceptible-Exposed-Infected-Recovered (SEIR) epidemiological model, there are terms at low order in the normal form transform which cause a significant difference between the average stochastic center manifold and the deterministic manifold [21]. Therefore, when working with the SEIR model, one must use the stochastic normal form coordinate transform approach to obtain the correct projection of the noise onto the center manifold.

Figure 5.8(a) compares the fraction of the population that is infected with a disease, I , computed using the complete, stochastic system of equations of the SEIR model with the time series of I computed using the reduced system of equations of the SEIR model that is based on the deterministic center manifold with a “naïve” replacement of the noise terms. One can see that the solution computed using the reduced system incorrectly predicts the time and amplitude of the initial outbreak and quickly becomes out of phase with the solution of the complete system. Although not shown, the poor agreement, in phase and amplitude, between the two solutions continues for long periods of time.

On the other hand, Fig. 5.8(b) compares the time series of I computed using

the complete, stochastic system of equations of the SEIR model with the time series of I computed using the reduced system of equations of the SEIR model that is found using the stochastic normal form coordinate transform. There is excellent agreement between the two solutions. The initial outbreak is successfully captured by the reduced system, and the reduced system continues to accurately predict the phase and amplitude of outbreaks over long periods of time.

The previous general analysis has been performed only for the 2D singularly perturbed Duffing system. Of interest is the application of the theory to more realistic stochastic dynamical systems. Beyond that, we plan to apply the theory to fully 3D systems as well as to actual oceanographic data.

Acknowledgments. We warmly thank M. Dykman for his insight and for introducing us to the optimal path theory. We also thank A.J. Roberts for his initial reading of the manuscript. The authors benefited from the comments and suggestions of anonymous reviewers. We gratefully acknowledge support from the Office of Naval Research, the Army Research Office, and the Air Force Office of Scientific Research. E.F. is supported by a National Research Council Research Associateship.

Appendix A. Escape Rate Using Stochastic (“Naïve”) Center Manifolds. Using the fourth-order stochastic (“naïve”) center manifold dynamical equation given by

$$(A.1) \quad \dot{x} = x - x^3 - \epsilon x + 2\epsilon^2 x - 5\epsilon^3 x + 4\epsilon x^3 + \sqrt{2D}\phi(t),$$

one finds that the escape rate from the attractor located at

$$x = x_a = \sqrt{(1 - \epsilon + 2\epsilon^2 - 5\epsilon^3)/(1 - 4\epsilon)}$$

to the saddle located at $x = x_s = 0$ is given as follows:

$$(A.2a) \quad W(\epsilon, D) = \frac{\sqrt{|U''(0)|U''(x_a)}}{2\pi} \exp(-\Delta U/D),$$

where

$$(A.2b) \quad U''(0) = -1 + \epsilon - 2\epsilon^2 + 5\epsilon^3,$$

$$(A.2c) \quad U''(x_a) = 2 - 2\epsilon + 4\epsilon^2 - 10\epsilon^3,$$

$$(A.2d) \quad \Delta U = |(-1 + 6\epsilon - 13\epsilon^2 + 34\epsilon^3 - 70\epsilon^4 + 76\epsilon^5 - 105\epsilon^6 + 100\epsilon^7) / [4(1 - 8\epsilon + 16\epsilon^2)]|.$$

Using the fifth-order stochastic (“naïve”) center manifold dynamical equation given by

$$(A.3) \quad \dot{x} = x - x^3 - \epsilon x + 2\epsilon^2 x - 5\epsilon^3 x + 4\epsilon x^3 + 14\epsilon^4 x - 20\epsilon^2 x^3 + \sqrt{2D}\phi(t),$$

one finds that the escape rate from the attractor located at

$$x = x_a = \sqrt{(1 - \epsilon + 2\epsilon^2 - 5\epsilon^3 + 14\epsilon^4)/(1 - 4\epsilon + 20\epsilon^2)}$$

to the saddle located at $x = x_s = 0$ is given as follows:

$$(A.4a) \quad W(\epsilon, D) = \frac{\sqrt{|U''(0)|U''(x_a)}}{2\pi} \exp(-\Delta U/D),$$

where

$$(A.4b) \quad U''(0) = -1 + \epsilon - 2\epsilon^2 + 5\epsilon^3 - 14\epsilon^4,$$

$$(A.4c) \quad U''(x_a) = 2 - 2\epsilon + 4\epsilon^2 - 10\epsilon^3 + 42\epsilon^4,$$

$$(A.4d) \quad \Delta U = \left| \left(1 - 2\epsilon + 5\epsilon^2 - 14\epsilon^3 + 42\epsilon^4 - 48\epsilon^5 + 81\epsilon^6 - 140\epsilon^7 + 196\epsilon^8 \right) / \left[4(-1 + 4\epsilon - 20\epsilon^2) \right] \right|.$$

Appendix B. Second Iteration Details. For this second iteration, we seek a correction to the x coordinate (slow process) with the form

$$(B.1a) \quad x = X + \xi(\tau, X, Y) + \dots,$$

$$(B.1b) \quad X' = F(\tau, X, Y) + \dots,$$

where ξ and F are small corrections. Substitution of Eqs. (3.17a)-(B.1b) into Eq. (3.12a) leads to

$$(B.2) \quad X' + \frac{\partial \xi}{\partial \tau} + \frac{\partial \xi}{\partial X} \frac{\partial X}{\partial \tau} + \frac{\partial \xi}{\partial Y} \frac{\partial Y}{\partial \tau} = \epsilon(Y + X - X^3) + \epsilon\sigma\phi.$$

Replacing $X' = \partial X/\partial \tau$ with F [Eq. (B.1b)], replacing $\partial Y/\partial \tau$ with $-Y$ [Eq. (3.17b)], and ignoring the term $\partial \xi/\partial X \cdot F$ since it is a product of small corrections gives the following equation:

$$(B.3) \quad F + \frac{\partial \xi}{\partial \tau} - Y \frac{\partial \xi}{\partial Y} = \epsilon(Y + X - X^3) + \epsilon\sigma\phi.$$

Equation (B.3) must now be solved for F and ξ . As in the first step, we employ principle (4) and keep the evolution equation [Eq. (B.1b)] as simple as possible. However, since the terms $\epsilon(X - X^3)$ located on the right-hand side of Eq. (B.3) do not contain τ or Y , these terms must be included in F . Therefore, one piece of F will be $F = \epsilon(X - X^3)$.

The remaining deterministic term on the right-hand side of Eq. (B.3) contains Y . This term can therefore be integrated into ξ . The equation to be solved is

$$(B.4) \quad -Y \frac{\partial \xi}{\partial Y} = \epsilon Y,$$

whose solution is given as $\xi = -\epsilon Y$.

To abide by principle (4), we would like to integrate the stochastic piece on the right-hand side of Eq. (B.3) into ξ , by solving the equation

$$(B.5) \quad \partial \xi/\partial \tau = \epsilon\sigma\phi.$$

However, the solution of Eq. (B.5) is given by

$$(B.6) \quad \xi = \epsilon\sigma \int \phi d\tau,$$

which has secular growth like a Wiener process. Since this would violate principle (1), we must let $F = \epsilon\sigma\phi$.

Putting the three pieces together yields $\xi = -\epsilon Y$ and $F = \epsilon(X - X^3) + \epsilon\sigma\phi$. Therefore, the new approximation of the coordinate transform and its dynamics are given by

$$(B.7a) \quad x = X - \epsilon Y + \mathcal{O}(\zeta^3),$$

$$(B.7b) \quad X' = \epsilon(X - X^3) + \epsilon\sigma\phi + \mathcal{O}(\zeta^3).$$

Appendix C. Third Iteration Details. To find the corrections, η and G , we substitute Eqs. (3.14a) and (3.14b) into Eq. (3.12b), which leads to the following equation:

$$(C.1) \quad G + \frac{\partial\eta}{\partial\tau} + \frac{\partial\eta}{\partial X} \frac{\partial X}{\partial\tau} - Y \frac{\partial\eta}{\partial Y} + \eta = x - x^3.$$

Substitution of the specific form of x given by Eq. (B.7a), the specific form of $X' = \partial X/\partial\tau$ given by Eq. (B.7b), and substitution of $\eta = X - X^3$ and $G = 0$ [see Eqs. (3.17a) and (3.17b)] into Eq. (C.1) gives one the following evolution equation driven by the updated residual of Eq. (3.12b):

$$(C.2) \quad \begin{aligned} G + \frac{\partial\eta}{\partial\tau} - Y \frac{\partial\eta}{\partial Y} + \eta = & \epsilon(-X - Y + 4X^3 - 3X^5 + 3X^2Y) \\ & + \epsilon\sigma(-\phi + 3X^2\phi) + \epsilon^2(-3XY^2) + \epsilon^3Y^3. \end{aligned}$$

We first consider the deterministic terms on the right-hand side of Eq. (C.2). Principle (4) is employed to keep the evolution equation [Eq. (3.14b)] as simple as possible, and since the terms $-\epsilon X$, $4\epsilon X^3$, $-3\epsilon X^5$ are not functions of τ or Y , we let $\eta = \epsilon(-X + 4X^3 - 3X^5)$. Consideration of the term $-3\epsilon^2 XY^2$ leads one to solve the following equation:

$$(C.3) \quad \eta - Y \frac{\partial\eta}{\partial Y} = -3\epsilon^2 XY^2.$$

The solution of Eq. (C.3) is $\eta = 3\epsilon^2 XY^2$.

The last deterministic terms on the right-hand side of Eq. (C.2) are $-\epsilon Y$ and $3\epsilon X^2 Y$. Since these two terms can't be integrated into η , they are included in G . The higher order term $\epsilon^3 Y^3$ will be ignored until a later iteration.

We now consider the stochastic terms on the right-hand side of Eq. (C.2). The equation to be solved is

$$(C.4) \quad \frac{\partial\eta}{\partial\tau} + \eta = -\epsilon\sigma\phi + 3\epsilon\sigma X^2\phi,$$

whose solution is given by

$$(C.5) \quad \eta = -\epsilon\sigma \int_{-\infty}^{\tau} \exp[-(\tau-s)]\phi(s) ds + 3\epsilon\sigma X^2 \int_{-\infty}^{\tau} \exp[-(\tau-s)]\phi(s) ds.$$

If we define

$$(C.6) \quad \int_{-\infty}^{\tau} \exp[-(\tau-s)]\phi(s) ds = e^{-\tau} * \phi,$$

then Eq. (C.5) can be written as follows:

$$(C.7) \quad \eta = -\epsilon\sigma e^{-\tau} * \phi + 3\epsilon\sigma X^2 e^{-\tau} * \phi.$$

Putting all of the η and G pieces from this third iteration together leads to the updated approximation of the coordinate transform and its evolution equation given by Eqs. (3.18a) and (3.18b).

Appendix D. Fourth Iteration Details. To find the corrections, ξ and F , we substitute Eqs. (B.1a) and (B.1b) into Eq. (3.12a), which leads to the following equation:

$$(D.1) \quad F + \frac{\partial\xi}{\partial\tau} + \frac{\partial\xi}{\partial X} \frac{\partial X}{\partial\tau} + \frac{\partial\xi}{\partial Y} \frac{\partial Y}{\partial\tau} = \epsilon y + \epsilon\sigma\phi.$$

Substitution of the specific forms of y [Eq. (3.18a)], $Y' = \partial Y/\partial\tau$ [Eq. (3.18b)], ξ [Eq. (B.7a)], and F [Eq. (B.7b)] into Eq. (D.1) leads to the following evolution equation driven by the updated residual of Eq. (3.12a):

$$(D.2) \quad F + \frac{\partial\xi}{\partial\tau} - Y \frac{\partial\xi}{\partial Y} = \epsilon^2 (-X + 4X^3 - 3X^5 - Y + 3X^2Y) + \epsilon^2\sigma (-e^{-\tau} * \phi + 3X^2 e^{-\tau} * \phi) + 3\epsilon^3 XY^2.$$

It is straightforward (and similar to what has been done in the previous iterations) to integrate the deterministic terms on the right-hand side of Eq. (D.2) into F and ξ .

Consideration of the stochastic terms on the right-hand side of Eq. (D.2) means that we must solve the following equation:

$$(D.3) \quad F + \frac{\partial\xi}{\partial\tau} = \epsilon^2\sigma (-e^{-\tau} * \phi + 3X^2 e^{-\tau} * \phi).$$

As in the second iteration, we can't integrate ϕ into ξ , since this would generate secular growth in violation of principle (1). Employing principle (5) to avoid a fast time convolution (memory integral) in the slow evolution F leads us to perform an integration by parts on each of the terms on the right-hand side of Eq. (D.3) so that

$$(D.4) \quad F + \frac{\partial\xi}{\partial\tau} = \epsilon^2\sigma [-\phi + e^{-\tau} * \phi' + 3X^2 (\phi - e^{-\tau} * \phi')].$$

It is clear that we now have $F = \epsilon^2\sigma(-\phi + 3X^2\phi)$ and $\xi = \epsilon^2\sigma(e^{-\tau} * \phi - 3X^2 e^{-\tau} * \phi)$.

Putting all of the ξ and F pieces from this fourth iteration together leads to the updated approximation of the coordinate transform and its evolution equation given

by Eqs. (3.19a) and (3.19b).

Appendix E. Normal Form Coordinate Transform.

$$\begin{aligned}
y = & Y + X - X^3 + \epsilon(-X + 4X^3 - 3X^5) + \epsilon\sigma(-e^{-\tau} * \phi + 3X^2e^{-\tau} * \phi) \\
& + \epsilon^2(2X - 20X^3 + 42X^5 + 3XY^2) \\
& + \epsilon^2\sigma(2e^{-\tau} * \phi + e^{-\tau} * e^{-\tau} * \phi - 18X^2e^{-\tau} * \phi - 12X^2e^{-\tau} * e^{-\tau} * \phi \\
& \quad + 24X^4e^{-\tau} * \phi + 15X^4e^{-\tau} * e^{-\tau} * \phi) \\
& + \epsilon^3(-X + 16X^3 - 66X^5 + 96X^7 - 45X^9 - 9XY^2 - Y^3/2 + 33X^3Y^2) \\
& + \epsilon^3\sigma(-e^{-\tau} * \phi + 18X^3Ye^{-\tau} * \phi - 6XYe^{-\tau} * \phi + 15X^2e^{-\tau} * \phi \\
& \quad + 45X^6e^{-\tau} * \phi - 51X^4e^{-\tau} * \phi + 18X^6e^{-\tau} * e^{-\tau} * \phi \\
& \quad - 24X^4e^{-\tau} * e^{-\tau} * \phi + 6X^2e^{-\tau} * e^{-\tau} * \phi + 3Y^2e^{+\tau} * \phi) \\
& + \epsilon^4(18X^5Y^2 - 6X^3Y^2 + 3Y^3/2 - 9Y^3X^2/2) \\
& + \epsilon^4\sigma(6XYe^{-\tau} * \phi + 54X^5Ye^{-\tau} * \phi - 36X^3Ye^{-\tau} * \phi + 9X^2Y^2e^{+\tau} * \phi \\
& \quad - 3Y^2e^{+\tau} * \phi + 3Y^2e^{+\tau} * e^{-\tau} * \phi - 9X^2Y^2e^{+\tau} * e^{-\tau} * \phi) \\
& + \epsilon^4\sigma^2\left(-3Xe^{-\tau} * (e^{-\tau} * \phi)^2 - 27X^5e^{-\tau} * (e^{-\tau} * \phi)^2\right. \\
\text{(E.1a)} \quad & \left. + 18X^3e^{-\tau} * (e^{-\tau} * \phi)^2\right) + \mathcal{O}(\zeta^4),
\end{aligned}$$

$$\begin{aligned}
Y' = & -Y + \epsilon(-Y + 3X^2Y) + \epsilon^2(Y - 6X^2Y + 9X^4Y) \\
& + \epsilon^3\sigma(6XY\phi - 18X^3Y\phi) \\
\text{(E.1b)} \quad & + \epsilon^4\sigma(-6XY\phi - 54X^5Y\phi + 36X^3Y\phi) + \mathcal{O}(\zeta^4),
\end{aligned}$$

$$\begin{aligned}
x = & X - \epsilon Y + \epsilon^2(Y - 3X^2Y) + \epsilon^2\sigma(e^{-\tau} * \phi - 3X^2e^{-\tau} * \phi) \\
& + \epsilon^3(6X^2Y - 12X^4Y - 2Y - 3XY^2/2) \\
& + \epsilon^4(-9X^6Y + 3X^4Y - 3X^2Y + Y + Y^3/6 + 9XY^2/2 - 33X^3Y^2/2) \\
& + \epsilon^5(-Y^3/2 + 3X^3Y^2 + 3X^2Y^3/2 - 9X^5Y^2) \\
& + \epsilon^3\sigma(-3e^{-\tau} * \phi - 33X^4e^{-\tau} * \phi + 24X^2e^{-\tau} * \phi - 15X^4e^{-\tau} * e^{-\tau} * \phi \\
& \quad - 6XYe^{+\tau} * \phi - e^{-\tau} * e^{-\tau} * \phi - 12X^2e^{-\tau} * e^{-\tau} * \phi) \\
& + \epsilon^4\sigma(e^{-\tau} * \phi - 15X^2e^{-\tau} * \phi - 6X^2e^{-\tau} * e^{-\tau} * \phi + 51X^4e^{-\tau} * \phi \\
& \quad - 45X^6e^{-\tau} * \phi + 24X^4e^{-\tau} * e^{-\tau} * \phi - 18X^6e^{-\tau} * e^{-\tau} * \phi \\
& \quad + 3XYe^{+\tau} * \phi + 3XYe^{-\tau} * \phi - 9X^3Ye^{+\tau} * \phi - 9X^3Ye^{-\tau} * \phi \\
& \quad - 3Y^2e^{+2\tau} * e^{+\tau} * \phi) \\
& + \epsilon^5\sigma(-54X^3Ye^{+\tau} * \phi + 9XYe^{+\tau} * \phi + 81X^5Ye^{+\tau} * \phi - 3XYe^{-\tau} * \phi \\
& \quad - 27X^5Ye^{-\tau} * \phi + 18X^3Ye^{-\tau} * \phi - 9X^2Y^2e^{+2\tau} * e^{+\tau} * \phi \\
& \quad + 3(Y^2e^{+2\tau} * e^{+\tau} * \phi) / 2 - 3(Y^2e^{+2\tau} * e^{-\tau} * \phi) / 2) \\
& + \epsilon^6\sigma(-6XYe^{+\tau} * \phi + 54X^3Ye^{+\tau} * \phi - 162X^5Ye^{+\tau} * \phi + 162X^7Ye^{+\tau} * \phi)
\end{aligned}$$

$$\begin{aligned}
& + \epsilon^5 \sigma^2 \left(3X (e^{-\tau} * \phi)^2 / 2 - 9X^3 (e^{-\tau} * \phi)^2 + 27X^5 (e^{-\tau} * \phi)^2 / 2 \right. \\
& \quad \left. + 3Xe^{-\tau} * (e^{-\tau} * \phi)^2 - 18X^3 e^{-\tau} * (e^{-\tau} * \phi)^2 \right. \\
\text{(E.1c)} \quad & \left. + 27X^5 e^{-\tau} * (e^{-\tau} * \phi)^2 \right) + \mathcal{O}(\zeta^4),
\end{aligned}$$

$$\begin{aligned}
X' = & \epsilon (X - X^3) + \epsilon \sigma \phi + \epsilon^2 (-X + 4X^3 - 3X^5) + \epsilon^2 \sigma (-\phi + 3X^2 \phi) \\
& + \epsilon^3 (2X - 20X^3 + 42X^5) \\
& + \epsilon^4 (-X + 16X^3 - 66X^5 - 96X^7 - 45X^9) \\
& + \epsilon^3 \sigma (3\phi - 24X^2 \phi + 33X^4 \phi) + \epsilon^4 \sigma (-\phi + 15X^2 \phi - 51X^4 \phi + 45X^6 \phi) \\
& + \epsilon^4 \sigma^2 (-6X \phi e^{-\tau} * \phi + 18X^3 \phi e^{-\tau} * \phi) \\
\text{(E.1d)} \quad & + \epsilon^5 \sigma^2 (-9X \phi e^{-\tau} * \phi + 54X^3 \phi e^{-\tau} * \phi - 81X^5 \phi e^{-\tau} * \phi) + \mathcal{O}(\zeta^4),
\end{aligned}$$

where

$$\text{(E.2)} \quad e^{+\tau} * \phi = \int_{\tau}^{+\infty} \exp[(\tau - s)] \phi(s) ds.$$

REFERENCES

- [1] L. ARNOLD, *Random Dynamical Systems*, Springer-Verlag, 1998.
- [2] L. ARNOLD AND P. IMKELLER, *Normal forms for stochastic differential equations*, Probab. Theory Rel., 110 (1998), pp. 559–588.
- [3] N. BERGLUND AND B. GENTZ, *Geometric singular perturbation theory for stochastic differential equations*, J. Differ. Equations, 191 (2003), pp. 1–54.
- [4] L. BILLINGS, E. M. BOLLT, AND I. B. SCHWARTZ, *Phase-space transport of stochastic chaos in population dynamics of virus spread*, Phys. Rev. Lett., 88 (2002), paper 234101.
- [5] E. M. BOLLT, L. BILLINGS, AND I. B. SCHWARTZ, *A manifold independent approach to understanding transport in stochastic dynamical systems*, Physica D, 173 (2002), pp. 153–177.
- [6] P. BOXLER, *A stochastic version of center manifold theory*, Probab. Theory Rel., 83 (1989), pp. 509–545.
- [7] J. CARR, *Applications of Centre Manifold Theory*, Springer-Verlag, 1981.
- [8] T. CARR, L. BILLINGS, I. SCHWARTZ, AND I. TRIANDAF, *Bi-instability and the global rate of unstable resonant orbits in a driven laser*, Physica D, 147 (2000), pp. 59–82.
- [9] P. H. COULLET, C. ELPHICK, AND E. TIRAPEGUI, *Normal form of a Hopf bifurcation with noise*, Phys. Lett. A, 111 (1985), pp. 277–282.
- [10] R. E. L. DEVILLE, E. VANDEN-EIJNDEN, AND C. B. MURATOV, *Two distinct mechanisms of coherence in randomly perturbed dynamical systems*, Phys. Rev. E, 72 (2005), paper 031105.
- [11] M. I. DYKMAN. Private communication.
- [12] M. I. DYKMAN, *Large fluctuations and fluctuational transitions in systems driven by coloured gaussian noise: A high-frequency noise*, Phys. Rev. A, 42 (1990), pp. 2020–2029.
- [13] M. I. DYKMAN AND B. GOLDING, *Controlling large fluctuations: Theory and experiment*, in Stochastic Processes in Physics, Chemistry, and Biology, J. A. Freund and T. Pöschel, eds., Springer-Verlag, 2000, pp. 365–377.
- [14] M. I. DYKMAN, P. V. E. MCCLINTOCK, V. N. SMELYANSKI, N. D. STEIN, AND N. G. STOCKS, *Optimal paths and the prehistory problem for large fluctuations in noise-driven systems*, Phys. Rev. Lett., 68 (1992), pp. 2718–2721.
- [15] M. I. DYKMAN, E. MORI, J. ROSS, AND P. M. HUNT, *Large fluctuations and optimal paths in chemical-kinetics*, J. Chem. Phys., 100 (1994), pp. 5735–5750.
- [16] M. I. DYKMAN, I. B. SCHWARTZ, AND A. S. LANDSMAN, *Disease extinction in the presence of random vaccination*, Phys. Rev. Lett., 101 (2008), paper 078101.

- [17] M. I. DYKMAN, I. B. SCHWARTZ, AND M. SHAPIRO, *Scaling in activated escape of underdamped systems*, Phys. Rev. E, 72 (2005), paper 021102.
- [18] S. J. B. EINHCOMB AND A. J. MCKANE, *Using path-integral methods to calculate noise-induced escape rates in bistable systems: The case of quasi-monochromatic noise*, in *Fluctuations and Order: The New Synthesis*, Mark Millonas, ed., Springer-Verlag, 1996, pp. 139–154.
- [19] C. C. ERIKSEN, T. J. OSSE, R. D. LIGHT, T. WEN, T. W. LEHMAN, P. L. SABIN, J. W. BALLARD, AND A. M. CHIOLDI, *Seaglider: A long-range autonomous underwater vehicle for oceanographic research*, IEEE J. Oceanic Eng., 26 (2001), pp. 424–436.
- [20] R. P. FEYNMAN AND A. R. HIBBS, *Quantum Mechanics and Path Integrals*, McGraw-Hill, Inc., 1965.
- [21] E. FORGOSTON, L. BILLINGS, AND I. B. SCHWARTZ, *Accurate time series prediction in reduced stochastic epidemic models*, 2009. submitted, available at preprint archive: <http://arxiv.org/abs/0903.1038>.
- [22] M. I. FREIDLIN, *On stable oscillations and equilibriums induced by small noise*, J. Stat. Phys., 103 (2001), pp. 283–300.
- [23] M. I. FREIDLIN AND A. D. WENTZELL, *Random Perturbations of Dynamical Systems*, Springer-Verlag, 1984.
- [24] L. GAMMAITONI, P. HÄNGGI, P. JUNG, AND F. MARCHESONI, *Stochastic resonance*, Rev. Mod. Phys., 70 (1998), pp. 223–287.
- [25] C. W. GARDINER, *Handbook of Stochastic Methods for Physics, Chemistry and the Natural Sciences*, Springer-Verlag, 2004.
- [26] R. GRAHAM AND T. TÉL, *Existence of a potential for dissipative dynamical systems*, Phys. Rev. Lett., 52 (1984), pp. 9–12.
- [27] J. HALES, A. ZHUKOV, R. ROY, AND M. I. DYKMAN, *Dynamics of activated escape and its observation in a semiconductor laser*, Phys. Rev. Lett., 85 (2000), pp. 78–81.
- [28] A. HAMM, T. TÉL, AND R. GRAHAM, *Noise-induced attractor explosions near tangent bifurcations*, Physics Letters A, 185 (1994), pp. 313–320.
- [29] J. A. HANSEN AND C. PENLAND, *Efficient approximate techniques for integrating stochastic differential equations*, Mon. Weather Rev., 134 (2006), pp. 3006–3014.
- [30] B. HAUSCHILDT, N. B. JANSON, A. BALANOV, AND E. SCHÖLL, *Noise-induced cooperative dynamics and its control in coupled neuron models*, Phys. Rev. E, 74 (2006), paper 051906.
- [31] G. HU, *Stationary solution of master-equations in the large-system-size limit*, Phys. Rev. A, 36 (1987), pp. 5782–5790.
- [32] S. K. HWANG, J. B. GAO, AND J. M. LIU, *Noise-induced chaos in an optically injected semiconductor laser model*, Phys. Rev. E, 61 (2000), pp. 5162–5170.
- [33] A. KAMENEV AND B. MEERSON, *Extinction of an infectious disease: A large fluctuation in a nonequilibrium system*, Phys. Rev. E, 77 (2008), paper 061107.
- [34] E. KNOBLOCH AND K. A. WIESENFELD, *Bifurcations in fluctuating systems: The center-manifold approach*, J. Stat. Phys., 33 (1983), pp. 611–637.
- [35] Y-C LAI, Z. LIU, L. BILLINGS, AND I. B. SCHWARTZ, *Noise-induced unstable dimension variability and transition to chaos in random dynamical systems*, Phys. Rev. E, 67 (2003), paper 026210.
- [36] D. G. LUCHINSKY, P. V. E. MCCLINTOCK, AND M. I. DYKMAN, *Analogue studies of nonlinear systems*, Rep. Prog. Phys., 61 (1998), pp. 889–997.
- [37] R. S. MAIER AND D. L. STEIN, *Escape problem for irreversible systems*, Phys. Rev. E, 48 (1993), pp. 931–938.
- [38] B. MEERSON. Private communication.
- [39] M. MILLONAS, ed., *Fluctuations and Order: The New Synthesis*, Springer-Verlag, 1996.
- [40] N. S. NAMACHCHIVAYA, *Stochastic bifurcation*, Appl. Math. Comput., 38 (1990), pp. 101–159.
- [41] N. S. NAMACHCHIVAYA AND Y. K. LIN, *Method of stochastic normal forms*, Int. J. Nonlinear Mech., 26 (1991), pp. 931–943.
- [42] A. J. ROBERTS, *Normal form transforms separate slow and fast modes in stochastic dynamical systems*, Physica A, 387 (2008), pp. 12–38.
- [43] W. RÜMELIN, *Numerical treatment of stochastic differential equations*, SIAM J. Numer. Anal., 19 (1982), pp. 604–613.
- [44] Z. SCHUSS AND A. SPIVAK, *Where is the exit point?*, Chem. Phys., 235 (1998), pp. 227–242.
- [45] I. B. SCHWARTZ, L. BILLINGS, AND E. M. BOLLT, *Dynamical epidemic suppression using stochastic prediction and control*, Phys. Rev. E, 70 (2004), paper 046220.
- [46] I. B. SCHWARTZ, L. BILLINGS, M. DYKMAN, AND A. LANDSMAN, *Predicting extinction rates in stochastic epidemic models*, J. Stat. Mech.-Theory E., (2009), paper P01005.
- [47] J. SHERMAN, R. E. DAVIS, W. B. OWENS, AND J. VALDES, *The autonomous underwater glider 'Spray'*, IEEE J. Oceanic Eng., 26 (2001), pp. 437–446.

- [48] D. C. WEBB, P. J. SIMONETTI, AND C. P. JONES, *Slocum: An underwater glider propelled by environmental energy*, IEEE J. Oceanic Eng., 26 (2001), pp. 447–452.
- [49] A.D. WENTZELL, *Rough limit theorems on large deviations for Markov stochastic processes, I*, Theor. Probab. Appl., 21 (1976), pp. 227–242.

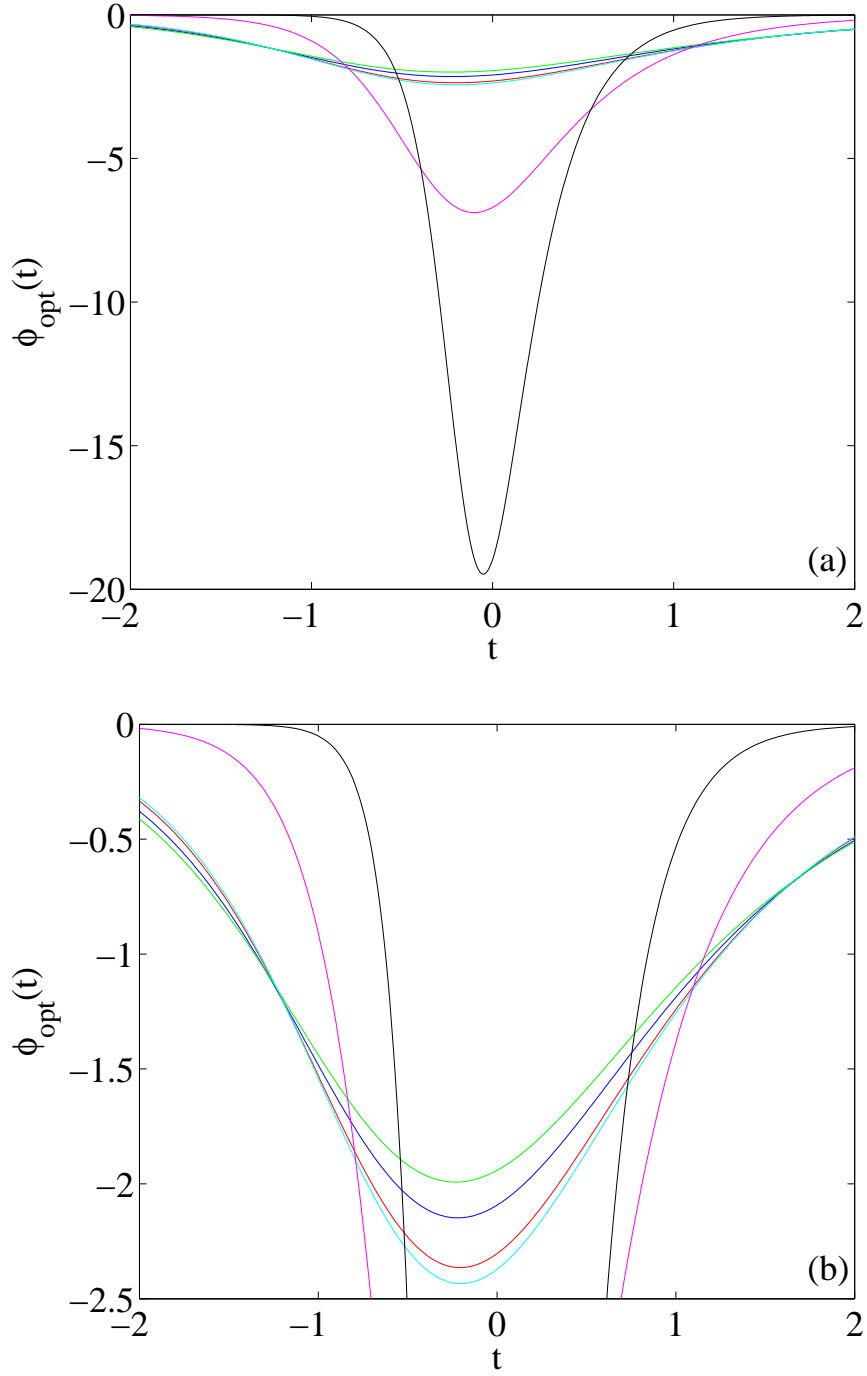


FIG. 5.1. (a) $\phi_{\text{opt}}(t)$ with $D = 0.05$ for $\epsilon = 0.02$ (red), $\epsilon = 0.1$ (blue), $\epsilon = 0.25$ (green), $\epsilon = 0.5$ (cyan), $\epsilon = 1.0$ (magenta), and $\epsilon = 1.5$ (black). (b) A close-up view of a section of Fig. 5.1(a).

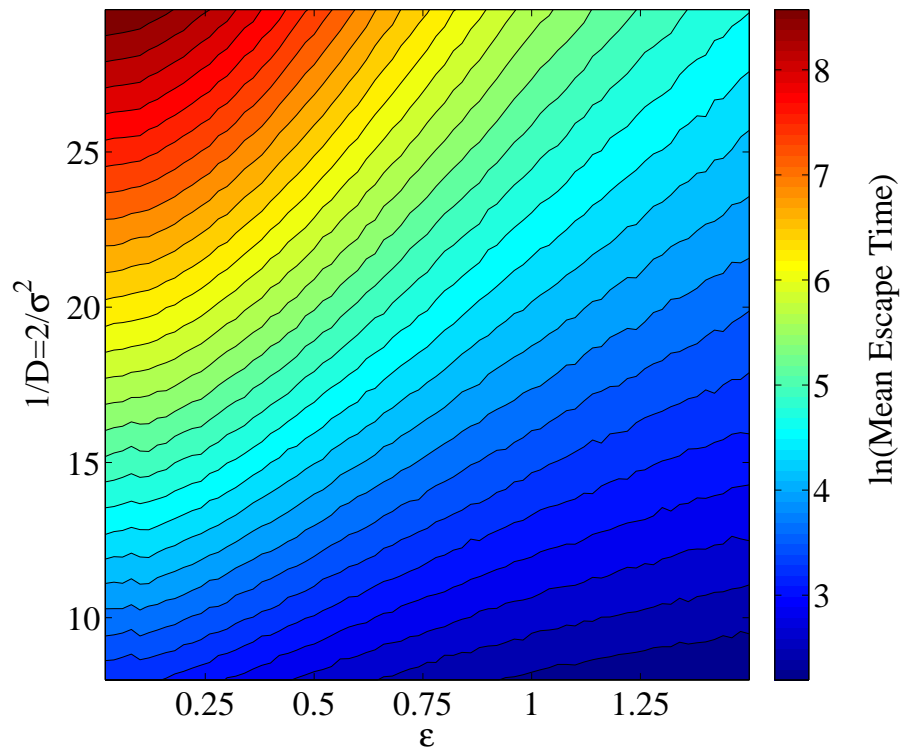


FIG. 5.2. Contours of numerically computed mean escape times (plotted as the natural log of the mean escape time) as a function of ϵ and $1/D$ for 10,000 particles.

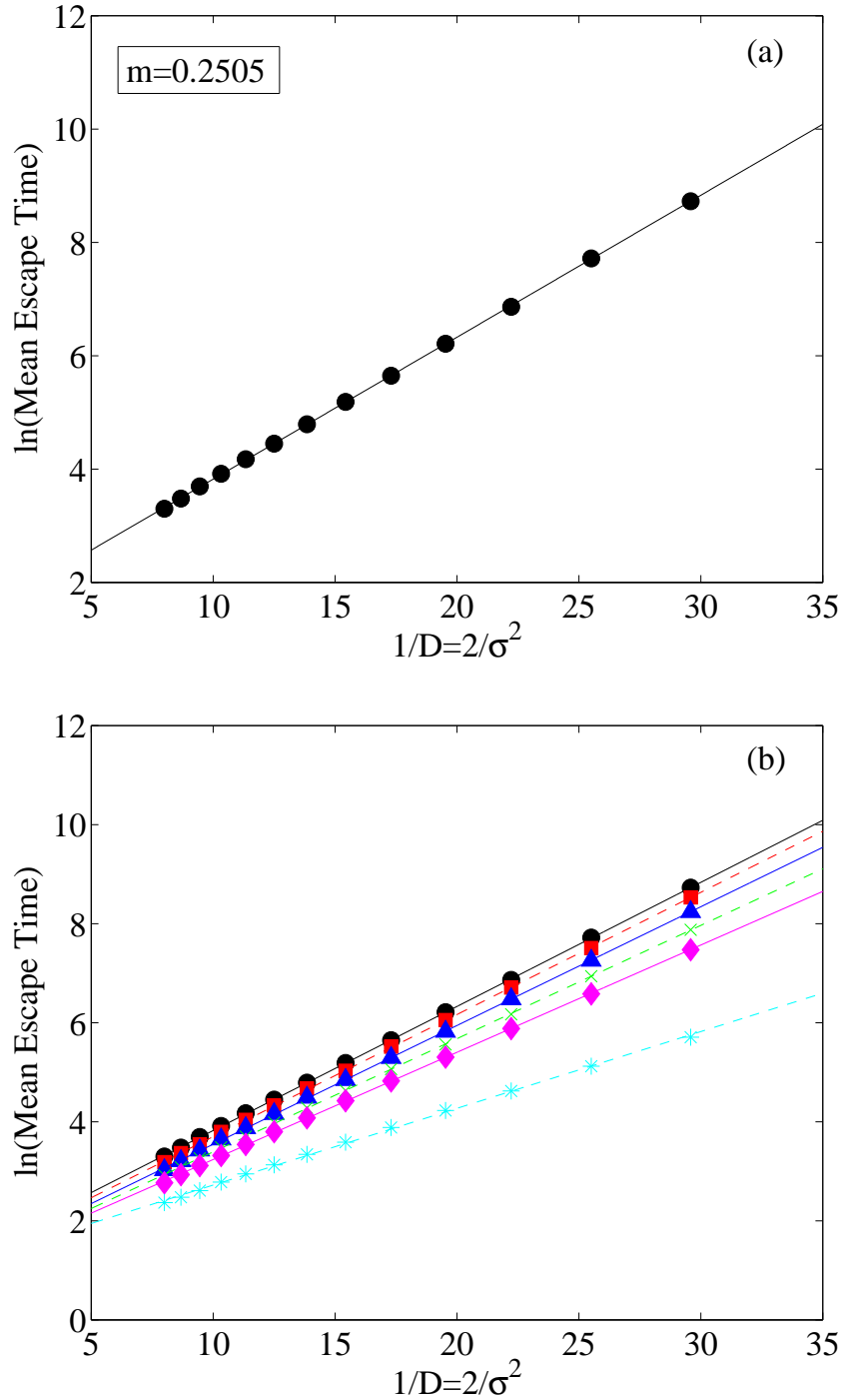


FIG. 5.3. (a) Vertical slice of Fig. 5.2 taken at $\epsilon = 0.1$. (b) Vertical slices of Fig. 5.2 taken at $\epsilon = 0.1$ (black, “circle” markers), $\epsilon = 0.2$ (red, “square” markers), $\epsilon = 0.3$ (blue, “triangle” markers), $\epsilon = 0.4$ (green, “cross” markers), $\epsilon = 0.5$ (magenta, “diamond” markers), and $\epsilon = 1.0$ (cyan, “asterisk” markers). The data points in both (a) and (b) are overlaid by a line of best fit.

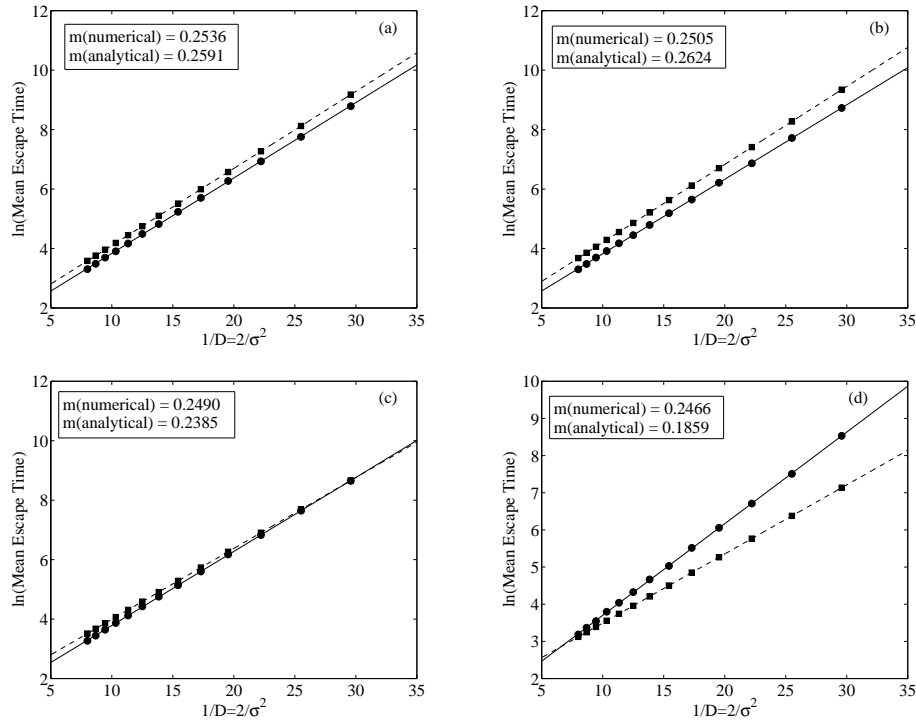


FIG. 5.4. Comparison of numerical data (“circle” markers) and linear fit (solid line) with analytical data (“square” markers) and linear fit (dashed line) of the natural log of the mean escape time as a function of $1/D$ for (a) $\epsilon = 0.02$, (b) $\epsilon = 0.1$, (c) $\epsilon = 0.14$, and (d) $\epsilon = 0.2$.

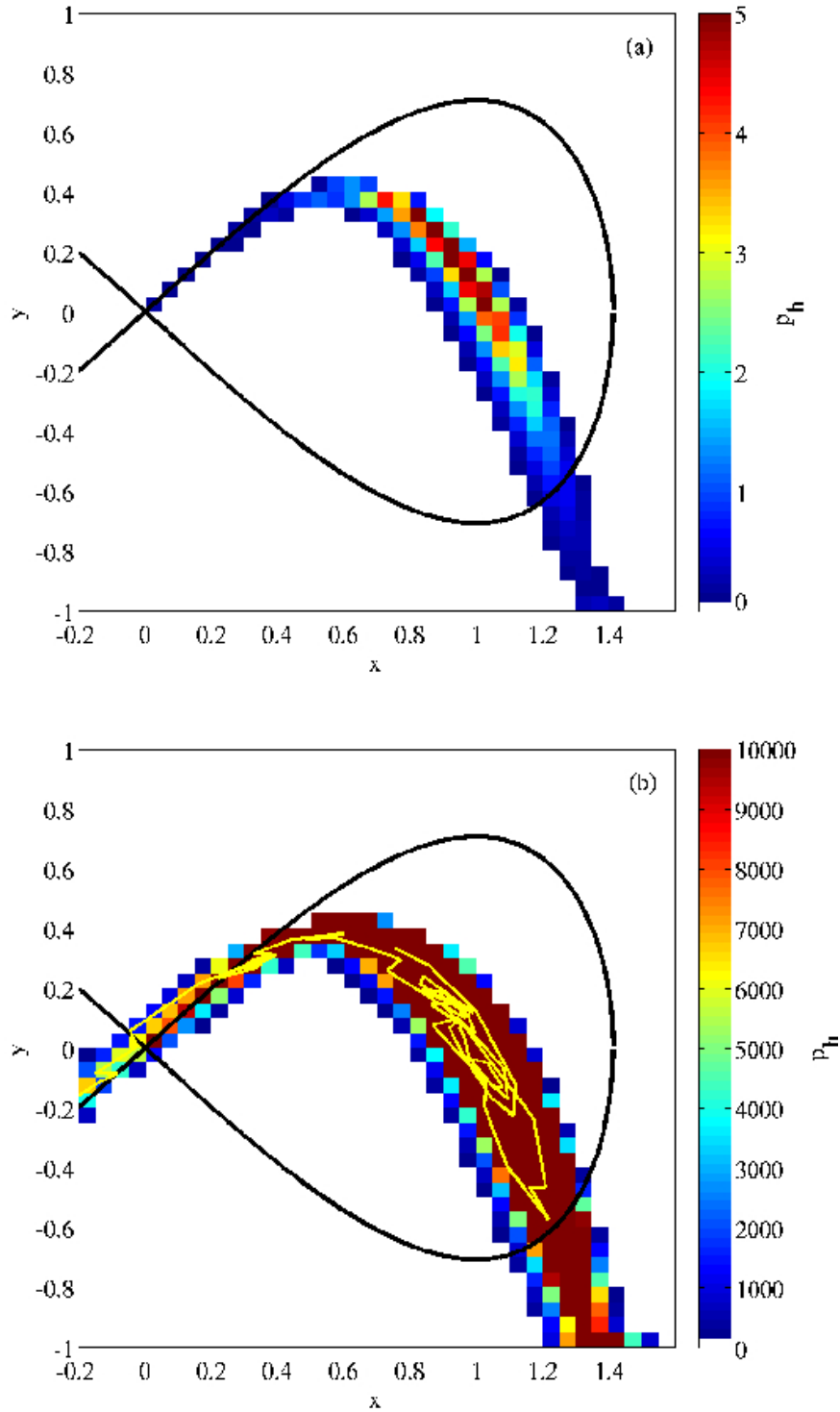


FIG. 5.5. (a) Histogram of escape path prehistory (for $t = 200$ of prehistory) of 10,000 particles with $\epsilon = 0.1$ and $\sigma = 0.3$. The color-bar values have been normalized by 10^5 , and the threshold 0 value is about 9000. (b) Same as Fig. 5.5(a), but with adjusted color-bar values, and including one particular particle's escape path prehistory (showing only $t = 50$ of prehistory).

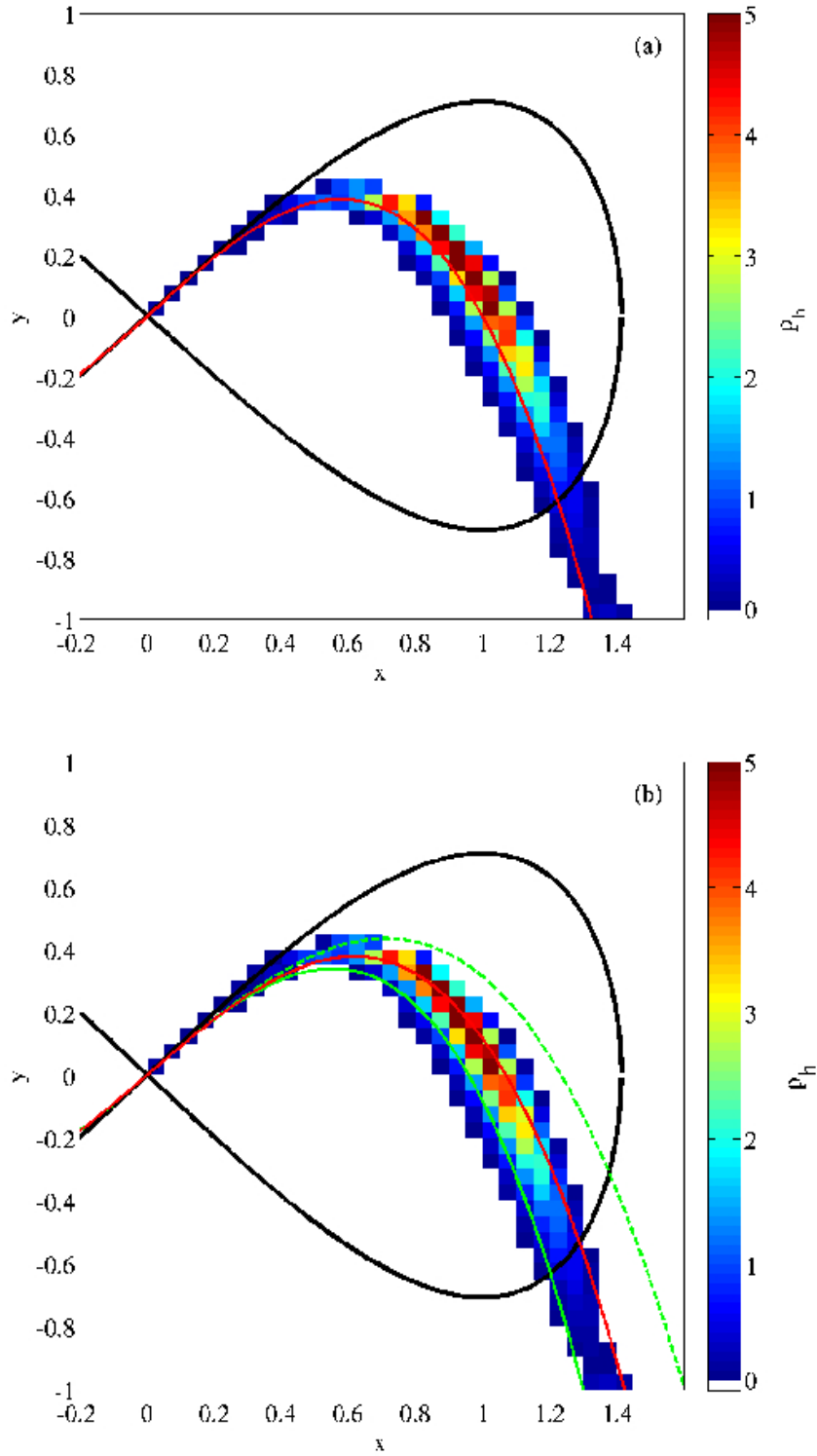


FIG. 5.6. Escape path prehistory histogram of Fig. 5.5(a) overlaid with (a) the graph of the slow manifold equation, and (b) the graphs of the third-order (solid, green line), fourth-order (dashed, green line), and fifth-order (solid, red line) center manifold equations given by Eq. (3.5a). For both Figs. 5.6(a) and 5.6(b), the color-bar values have been normalized by 10^5 , and the threshold 0 value is about 9000.

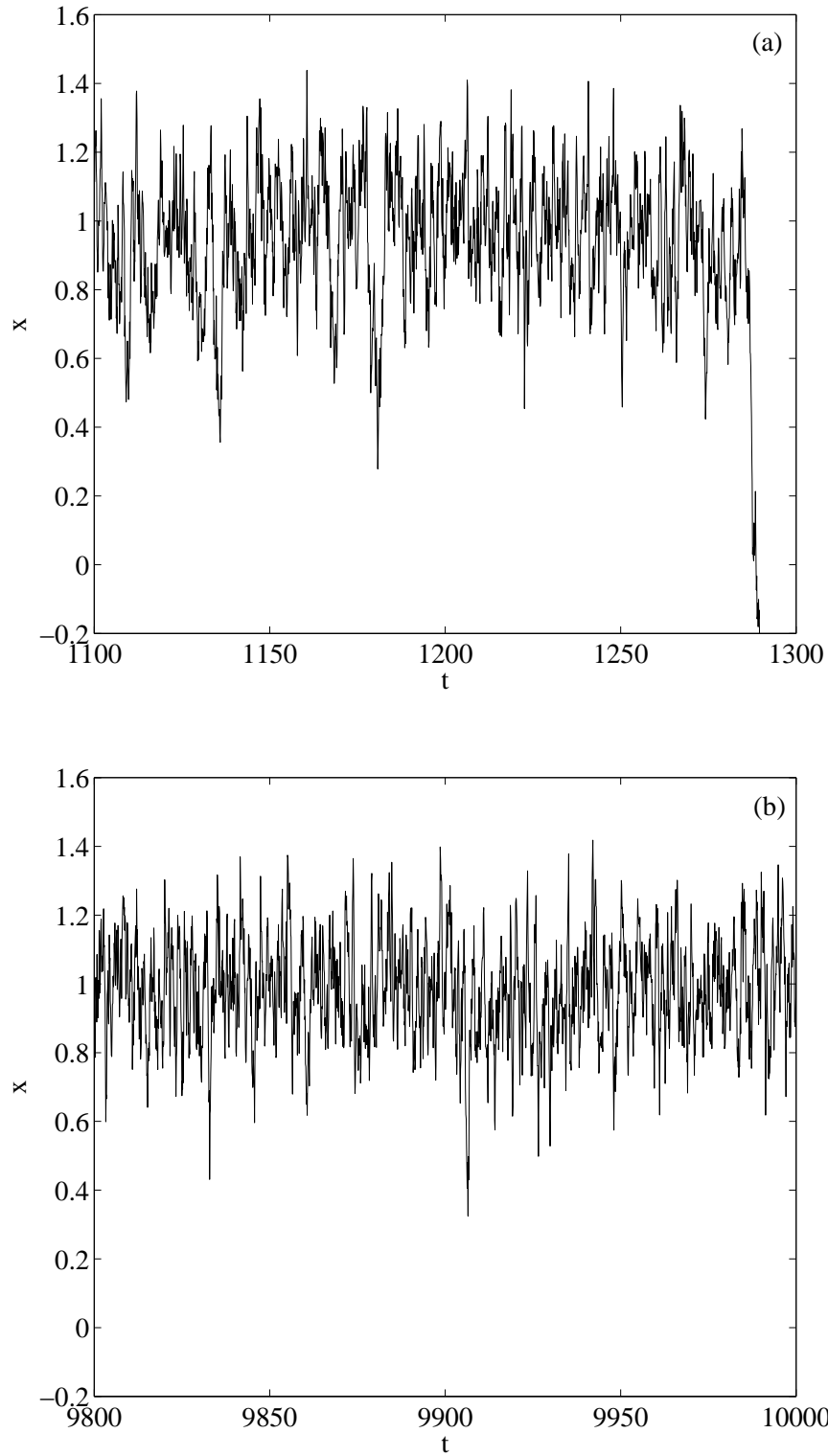


FIG. 5.7. Location of a particle (x coordinate) as a function of time t (a) without control, and (b) with control.

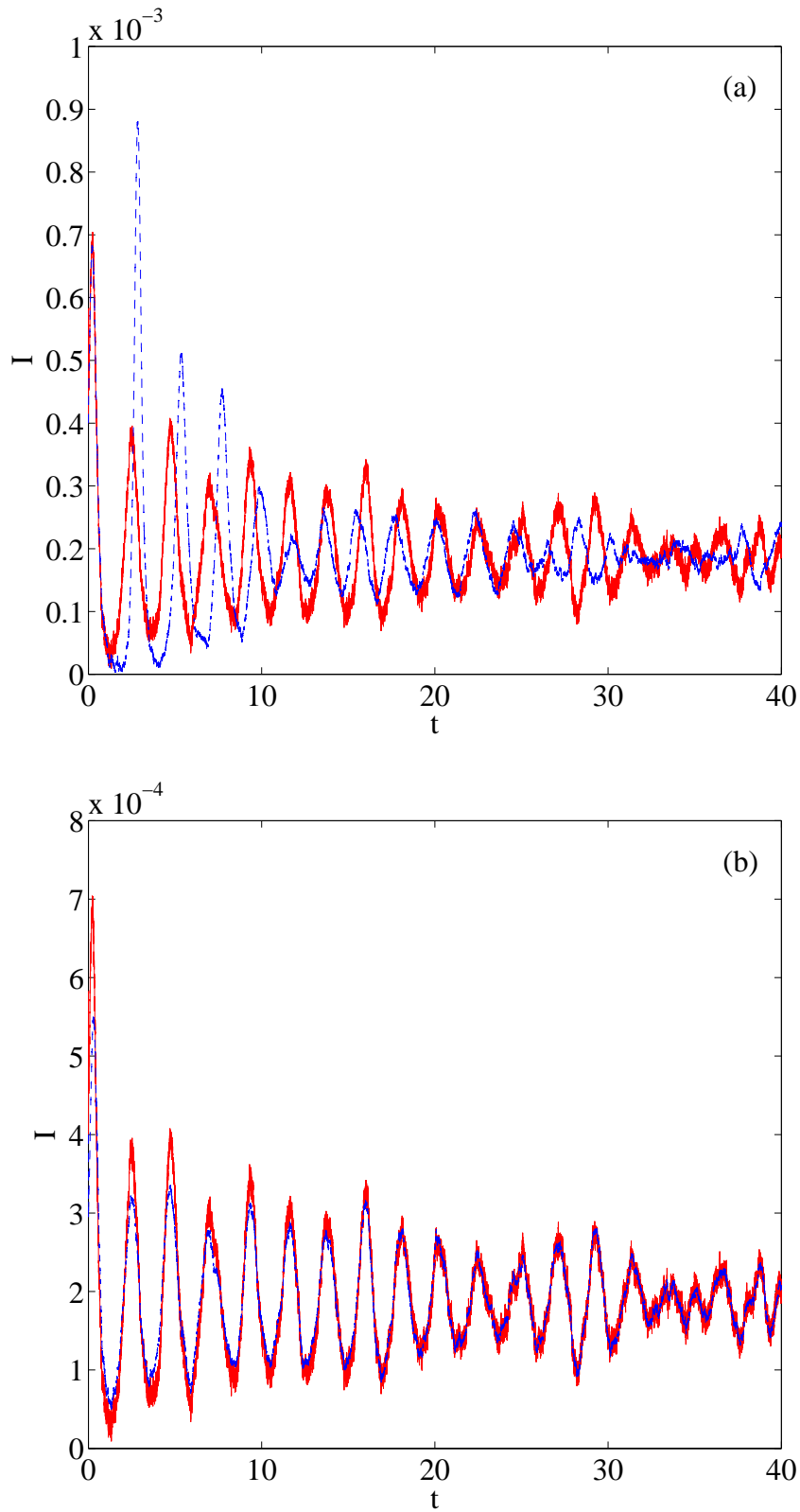


FIG. 5.8. Time series of the fraction of the population that is infected with a disease, I , computed using the complete, stochastic system of equations of the SEIR model (red, solid line), and (a) computed using the reduced system of equations of the SEIR model that is based on the deterministic center manifold with a “naïve” replacement of the noise terms (blue, dashed line), and (b) computed using the reduced system of equations of the SEIR model that is found using the stochastic normal form coordinate transform (blue, dashed line).